

# Tuning the Decay Time of Lanthanide-Based Near Infrared Luminescence from Micro- to Milliseconds through d→f Energy Transfer in Discrete Heterobimetallic Complexes

Stéphane Torelli,<sup>[a]</sup> Daniel Imbert,<sup>[b]</sup> Martine Cantuel,<sup>[a]</sup> Gérald Bernardinelli,<sup>[c]</sup> Sandra Delahaye,<sup>[d]</sup> Andreas Hauser,<sup>[d]</sup> Jean-Claude G. Bünzli,<sup>\*[b]</sup> and Claude Piguet<sup>\*[a]</sup>

**Abstract:** Inert and optically active pseudo-octahedral Cr<sup>III</sup>N<sub>6</sub> and Ru<sup>II</sup>N<sub>6</sub> chromophores have been incorporated by self-assembly into heterobimetallic triple-stranded helicates *HHH*-[CrLnL<sub>3</sub>]<sup>6+</sup> and *HHH*-[RuLnL<sub>3</sub>]<sup>5+</sup>. The crystal structures of [CrLnL<sub>3</sub>](CF<sub>3</sub>SO<sub>3</sub>)<sub>6</sub> (Ln=Nd, Eu, Yb, Lu) and [RuLnL<sub>3</sub>](CF<sub>3</sub>SO<sub>3</sub>)<sub>5</sub> (Ln=Eu, Lu) demonstrate that the helical structure can accommodate metal ions of different sizes, without sizeable change in the intermetallic

M···Ln distances. These systems are ideally suited for unravelling the molecular factors affecting the intermetallic *nd*→*4f* communication. Visible irradiation of the Cr<sup>III</sup>N<sub>6</sub> and Ru<sup>II</sup>N<sub>6</sub> chromophores in *HHH*-[MLnL<sub>3</sub>]<sup>5/6+</sup> (Ln=

Nd, Yb, Er; M=Cr, Ru) eventually produces lanthanide-based near infrared (NIR) emission, after directional energy migration within the complexes. Depending on the kinetic regime associated with each specific d–f pair, the NIR luminescence decay times can be tuned from micro- to milliseconds. The origin of this effect, together with its rational control for programming optical functions in discrete heterobimetallic entities, are discussed.

**Keywords:** energy transfer · helicates · heterobimetallic complexes · lanthanides · near infrared luminescence

## Introduction

Although long-lived visible Eu<sup>III</sup> and Tb<sup>III</sup> emitters have been systematically exploited in the time-resolved separation of the target signal from the fluorescent background in bioassays,<sup>[1]</sup> the development of alternative near infrared (NIR) trivalent lanthanide probes (Ln=Pr, Nd, Er, Yb) is recent,<sup>[2–7]</sup> despite the transparency of biological tissues in this spectral range.<sup>[8]</sup> Moreover, the lower energy of the excited states in NIR emitters is compatible with visible sensitization processes outside the range of biological absorption, thus offering perspectives for improved detection limits.<sup>[9]</sup> Lanthanide-based NIR emitters are also used for optical amplification in lasers<sup>[10]</sup> and silica-based fiber optic networks, for which the emission wavelengths (1330 nm for Pr<sup>III</sup> and 1550 nm for Er<sup>III</sup>) match the “window of transparency” in silica used for telecommunication.<sup>[11]</sup> Potential applications are thus obvious, but designing efficient sensitization for lanthanide-based NIR emitters remains a challenge, because the Laporte-forbidden 4f→4f transitions prevent direct excitation of the photoluminescence.<sup>[10]</sup> For Pr<sup>III</sup>, Nd<sup>III</sup>, and Er<sup>III</sup>, the plethora of accessible excited levels in the 6000–35000 cm<sup>-1</sup> range is compatible with indirect sensitization processes, during which a suitable aromatic chromo-

[a] Dr. S. Torelli, M. Cantuel, Prof. Dr. C. Piguet  
Department of Inorganic, Analytical and Applied Chemistry  
University of Geneva  
30 quai E. Ansermet, 1211 Geneva 4 (Switzerland)  
Fax: (+41)22-379-6830  
E-mail: claude.piguet@chiam.unige.ch

[b] Dr. D. Imbert, Prof. Dr. J.-C. G. Bünzli  
Laboratory of Lanthanide Supramolecular Chemistry  
Ecole Polytechnique Fédérale de Lausanne (EPFL)  
BCH 1402, 1015 Lausanne (Switzerland)  
Fax: (+41)21-693-9825  
E-mail: jean-claude.bunzli@epfl.ch

[c] Dr. G. Bernardinelli  
Laboratory of X-ray Crystallography  
University of Geneva  
24 quai E. Ansermet, 1211 Geneva 4 (Switzerland)

[d] S. Delahaye, Prof. Dr. A. Hauser  
Department of Physical Chemistry  
University of Geneva  
24 quai E. Ansermet, 1211 Geneva 4 (Switzerland)

Supporting information (analytical data, additional tables (Tables S1–S14) and figures (Figure S1–S8) for structural and spectroscopic analyses) for this article is available on the WWW under <http://www.chemeurj.org/> or from the author.

phore is irradiated in the UV<sup>[2]</sup> or visible<sup>[3]</sup> spectral range, followed by Ligand→Ln<sup>III</sup> energy transfer. Since the spectral overlap between the broad ligand emission spectrum (i.e., donor) and the Ln-centered narrow line absorption spectrum (i.e., acceptor) is considerable, the classical Förster–Dexter mechanism<sup>[12]</sup> holds for modeling these energy transfer processes. For Yb<sup>III</sup>, the existence of a single and sharp <sup>2</sup>F<sub>5/2</sub> excited level around 10000 cm<sup>-1</sup> strongly limits direct spectral overlap, but the efficient sensitization of the Yb(<sup>2</sup>F<sub>5/2</sub>→<sup>2</sup>F<sub>7/2</sub>) emission by high-energy ligand chromophores has been assigned to alternative electron transfer pathways (via Yb<sup>II</sup>),<sup>[2b,13]</sup> and/or phonon-assisted processes.<sup>[2a]</sup> The possible simultaneous occurrence of these different mechanisms in the same complex, combined with the extreme difficulty to separate exchange from multipolar contributions in Ligand→Ln<sup>III</sup> energy transfer, limit the molecular programming and tuning of NIR luminescence.<sup>[14]</sup> In this context, the alternative use of a d-block complex as a donor, well-separated from the lanthanide acceptor, offers the potential for a rational approach, since multipolar electrostatic interactions (with or without phonon-assistance) become the only vectors for intramolecular *nd*→4*f* energy transfer processes.<sup>[10,12–14]</sup> The first systems matching this criterion took advantage of the intense charge-transfer transitions, often mixed with d–d transitions, occurring in the visible spectral range of redox-active d-block complexes, to efficiently collect photonic energy. Intersystem crossing (isc) followed by multipolar *nd*→4*f* energy transfer complete the energy funneling processes leading to the lanthanide-based NIR emission.<sup>[4–7]</sup> The well-known [Ru<sup>II</sup>(2,2'-bipyridine)<sub>3</sub>]<sup>2+</sup> chromophore (efficient <sup>1</sup>MLCT absorption centered at 22170 cm<sup>-1</sup>, followed by the quantitative isc feeding of the <sup>3</sup>MLCT state)<sup>[15]</sup> has been integrated into polymetallic d–f complexes containing Ln<sup>III</sup>-centered NIR emitters, and efficient intramolecular Ru(<sup>3</sup>MLCT)→Ln<sup>III</sup> (Ln=Nd, Er, Yb) energy transfer processes have been evidenced.<sup>[4]</sup> Other work has focused on square-planar Pt<sup>II</sup> centers,<sup>[5]</sup> and pseudo-octahedral Re<sup>II</sup><sup>[6]</sup> and Cr<sup>III</sup><sup>[7]</sup> building blocks, but kinetic rate constants, *k*<sub>ET</sub><sup>M,Ln</sup>, for *nd*→4*f* energy transfers in discrete heterometallic complexes have only been reported for Ru<sup>II</sup>→Nd<sup>III</sup> transfer in complexes **1**<sup>[4a]</sup> and **2**,<sup>[4b]</sup> Ru<sup>II</sup>→Yb<sup>III</sup> transfer in **1**,<sup>[4a]</sup> and Pt<sup>II</sup>→Ln<sup>III</sup> (Ln=Nd, Er, Yb) transfer in **3** and **4** (Figure 1).<sup>[5a,b]</sup>

Owing to the large intermetallic distances (≥ 7–8 Å, Figure 1), the mathematical multipolar expansion can be reasonably limited to the first dipole–dipolar term, and the efficiency of the *nd*→4*f* energy transfer process (*η*<sub>ET</sub><sup>M,Ln</sup>) is given by Equation (1).<sup>[16]</sup>

$$\eta_{\text{ET}}^{\text{M,Ln}} = \frac{k_{\text{ET}}^{\text{M,Ln}}}{k_{\text{lum}}^{\text{M}} + k_{\text{ET}}^{\text{M,Ln}}} = \frac{k_{\text{ET}}^{\text{M,Ln}}}{k_{\text{obs}}^{\text{M}}} = \frac{1}{1 + (R_{\text{DA}}^{\text{M,Ln}}/R_0^{\text{M,Ln}})^6} \quad (1)$$

*k*<sub>lum</sub><sup>M</sup> is the decay rate constant of the donor d-block chromophore (M) in the absence of an acceptor (Ln), *R*<sub>DA</sub><sup>M,Ln</sup> is the distance between the donor and the acceptor, and *R*<sub>0</sub><sup>M,Ln</sup> is the so-called critical distance for 50% energy transfer, which can be estimated with Equation (2).

$$(R_0^{\text{M,Ln}})^6 = 8.75 \times 10^{-25} \kappa^2 \Phi_{\text{F}} n^{-4} J \text{ [cm}^6\text{]} \quad (2)$$

*κ*<sup>2</sup> is an orientation factor having an isotropic limit of 2/3, *Φ*<sub>F</sub> is the quantum yield of the donor luminescence in absence of acceptor, *n* is the refractive index of the intermetallic medium, and *J* is the overlap integral between the emission spectrum of the donor and the absorption spectrum of the acceptor (in cm<sup>6</sup> mol<sup>-1</sup>). The considerable number of parameters affecting *k*<sub>ET</sub><sup>M,Ln</sup>, combined with their dependence on molecular and electronic structures, have dissuaded the rational programming of intermetallic energy transfer in semi-flexible polymetallic d–f complexes, and the search for efficient d-block sensitizers entirely relies on empiric investigations.

To address which factors are the most pertinent for controlling *nd*→4*f* energy transfers, we have connected the inert donors [Cr<sup>III</sup>(2-benzimidazolpyridine)<sub>3</sub>]<sup>3+</sup> and [Ru<sup>II</sup>(2-benzimidazolpyridine)<sub>3</sub>]<sup>2+</sup> to pseudo-tricapped trigonal-prismatic Ln<sup>III</sup>N<sub>6</sub>O<sub>3</sub> chromophores in the C<sub>3</sub>-symmetrical triple-stranded helicates *HHH*-[MLnL<sub>3</sub>]<sup>5/6+</sup> (*HHH* stands for *head-to-head-to-head*, Figure 2).<sup>[17–19]</sup>

The rigidity of the triple helix fixes the intermetallic distance (9.0–9.3 Å) for any d–f pair, which 1) restricts the number of parameters (i.e., *R*<sub>DA</sub><sup>M,Ln</sup> is roughly invariant), and 2) ensures that the dipole-dipolar mechanism holds. Preliminary data collected for *HHH*-[CrLnL<sub>3</sub>]<sup>6+</sup> (Ln=Nd, Yb) point to unusually slow energy transfer *k*<sub>ET</sub><sup>Cr,Nd</sup>=1.8×10<sup>3</sup> s<sup>-1</sup> and *k*<sub>ET</sub><sup>Cr,Yb</sup>=2.2×10<sup>2</sup> s<sup>-1</sup>,<sup>[18]</sup> which are three orders of magnitude lower than those reported for analogous RuLn complexes (Figure 1). Herein, we focus on the detailed structural variations induced by the accommodation of different metal ions (M=Cr, Ru; Ln=Nd, Eu, Er, Yb, Lu) within the triple helices, and their consequences for *nd*→4*f* energy transfer. A quantitative kinetic model leads to a set of criteria, which can be rationally used for tuning the lifetimes of the lanthanide-based NIR emission.

## Results and Discussion

**Self-assembly of the inert d–f triple-stranded helicates *HHH*-[CrLnL<sub>3</sub>]<sup>6+</sup> (Ln=Nd, Gd, Yb) and *HHH*-[RuLnL<sub>3</sub>]<sup>5+</sup> (Ln=Nd, Eu, Gd, Er, Yb):** Since thermodynamically controlled assemblies leading to the final heterobimetallic helicates require labile metal ions,<sup>[20]</sup> the introduction of inert Cr<sup>III</sup> and Ru<sup>II</sup> requires special conditions. For Cr<sup>III</sup>, we have taken advantage of the lability of its reduced Cr<sup>II</sup> form to assemble *HHH*-[Cr<sup>III</sup>LnL<sub>3</sub>]<sup>5+</sup>, prior to aerobic oxidation<sup>[17]</sup> leading to [CrLnL<sub>3</sub>](CF<sub>3</sub>SO<sub>3</sub>)<sub>6</sub>·*x*H<sub>2</sub>O (Ln=Gd, Nd: *x*=6; Ln=Yb: *x*=4, Figure 2) in fair yields (58–67%, see Table S1 in the Supporting Information). Since the [Ru<sup>III</sup>(2-benzimidazolpyridine)<sub>3</sub>]<sup>3+</sup> entity is too oxidizing and kinetically inert to be used as a precursor, we have resorted to the recently reported labilizing effect of polar solvents on [Ru<sup>II</sup>(α,α'-diimine)<sub>3</sub>]<sup>2+</sup>.<sup>[19]</sup> Self-assembly of L (3 equiv) with [Ru(DMSO)<sub>5</sub>(H<sub>2</sub>O)]<sup>2+</sup> (1 equiv) and Ln<sup>III</sup> (1 equiv) in ethanol under reflux, followed by recrystallization from metha-

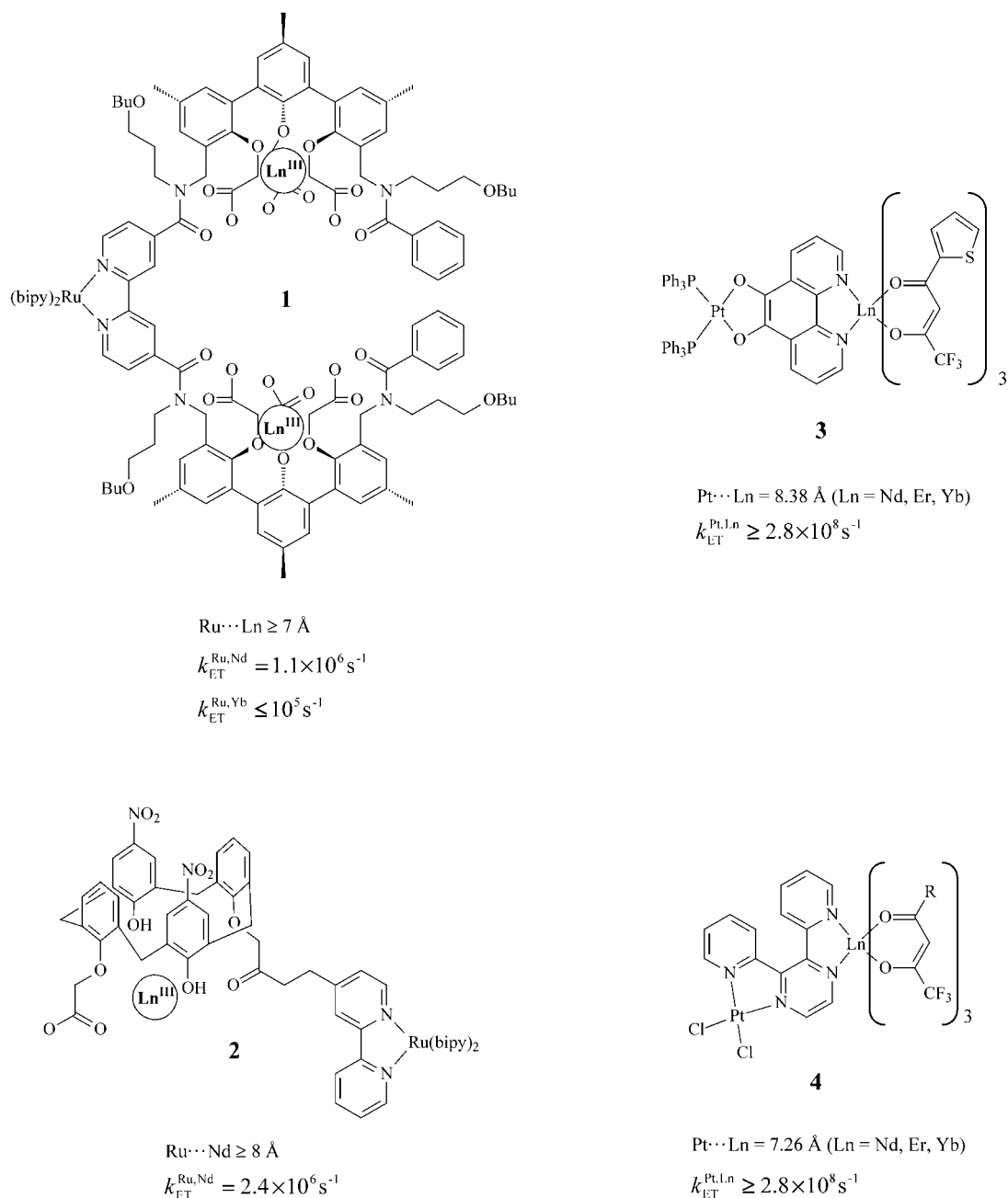


Figure 1. Molecular structures of discrete heterometallic d-f complexes **1–4**, for which the rate constant of intermetallic energy transfer ( $k_{ET}^{M,Ln}$ ) has been reported (295 K, see text for references).

no/diethyl ether, indeed produces 63–70% of  $[RuLnL_3](CF_3SO_3)_5 \cdot x H_2O \cdot y CH_3OH$  (Ln = Nd:  $x = 10$ ,  $y = 1$ ; Ln = Eu:  $x = 2$ ,  $y = 2$ ; Ln = Gd, Er, Yb:  $x = 6$ ,  $y = 1$ ; see Figure 2, and Table S1 in the Supporting Information). For photophysical comparisons, the related labile helicates  $[ZnLnL_3](CF_3SO_3)_5 \cdot 3 H_2O$  (Ln = Nd, Yb; Table S1) are obtained by the simple mixing of L (3 equiv) with  $Zn^{2+}$  (1 equiv) and  $Ln^{III}$  (1 equiv) in acetonitrile.<sup>[21]</sup> X-ray quality prisms were obtained by slow diffusion of diethylether into concentrated acetonitrile solutions for  $[CrNdL_3](CF_3SO_3)_6(CH_3CN)_4 \cdot (H_2O)$  (**5**) and  $[CrYbL_3](CF_3SO_3)_6(CH_3CN)_4$  (**7**), while

layering pentane onto a methanolic solution of the ruthenium complexes gives  $[RuEuL_3](CF_3SO_3)_5(CH_3OH)_{1.5}(H_2O)$  (**9**). For the sake of simplicity, the heterobimetallic cationic helicates  $HHH-[Cr^{III}LnL_3]^{6+}$ ,  $HHH-[Ru^{II}LnL_3]^{5+}$ , and  $HHH-[Zn^{II}LnL_3]^{5+}$  will often be termed CrLn, RuLn, and ZnLn in the following discussion.

**Crystal and molecular structures of  $[CrNdL_3](CF_3SO_3)_6 \cdot (CH_3CN)_4(H_2O)$  (**5**) and  $[CrLnL_3](CF_3SO_3)_6(CH_3CN)_4$  (Ln = Eu, **6**; Ln = Yb, **7** and Ln = Lu, **8**):** The two crystal structures CrNd (**5**) and CrYb (**7**)<sup>[18]</sup> are isostructural with

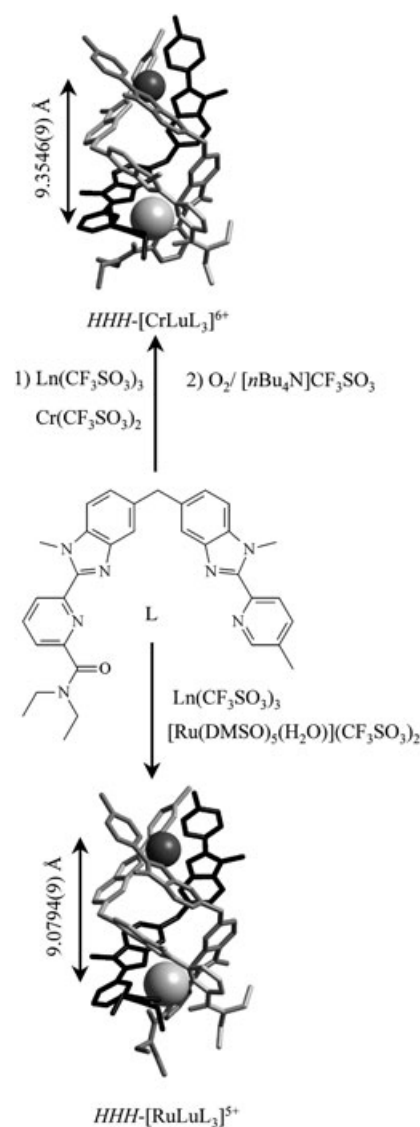


Figure 2. Self-assembly and crystal structures of  $HHH-[CrLuL_3]^{6+}$ <sup>[17]</sup> and  $HHH-[RuLuL_3]^{5+}$ .<sup>[19]</sup>

CrEu (**6**) and CrLu (**8**) previously described.<sup>[17]</sup> Each crystal structure comprises discrete triple-helical cations  $HHH-[Cr^{III}LnL_3]^{6+}$ , six ionic triflate anions, and four non-coordinated acetonitrile molecules. In **5**, the larger ionic size of  $Nd^{III}$  provides enough voids for the incorporation of an additional disordered water molecule in the unit cell, without significantly affecting the cell parameters. The atomic numbering scheme is shown in Figure 3a, while a view of the triple-helical cation is given in Figure 3b. The geometrical data are collected in Table 1 and in Tables S2–S5 in the Supporting Information.

The four triple-helical cations  $HHH-[CrLnL_3]^{6+}$  ( $Ln = Nd, Eu, Yb, Lu$ ) are superimposable (see Figure S1 in the Supporting Information), except for the expected faint contraction of the nine-coordinate lanthanide radii along the series.<sup>[22]</sup> The experimental six-coordinate  $Cr^{III}$  ionic radii, calculated by using Shannon's definition with  $r(N) = 1.46 \text{ \AA}$ ,

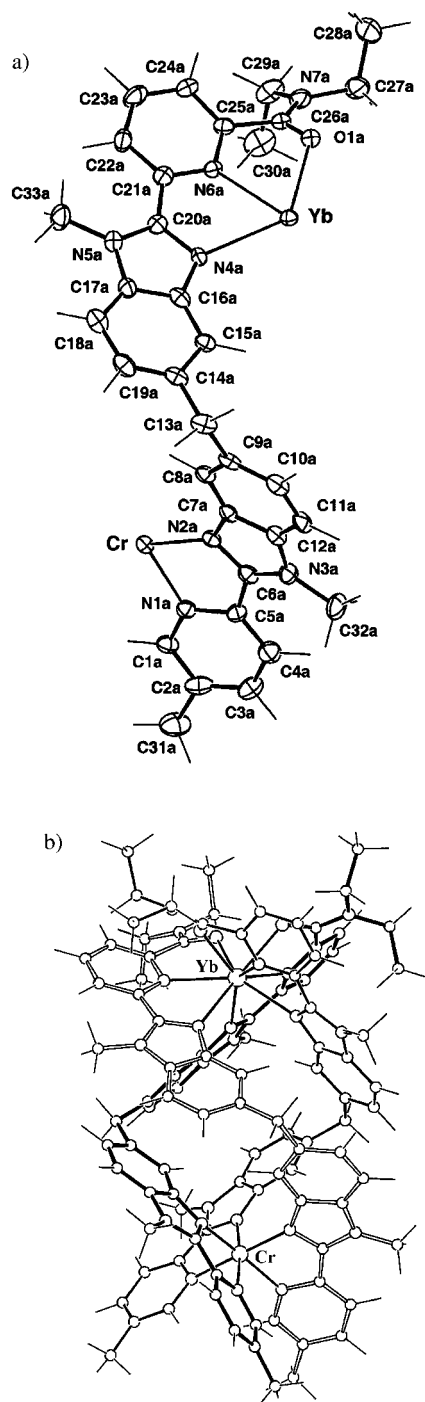


Figure 3. a) Numbering scheme for the cation  $HHH-[CrLnL_3]^{6+}$  in **5–10** (indices b and c correspond to the other strands; ellipsoids are represented at 40% probability level). b) Projection of  $HHH-[CrLnL_3]^{6+}$  perpendicular to the *pseudo*- $C_3$  axis. The CrYb complex is represented as a specimen.

amount to  $R_{Cr}^{CN=6} = 0.585\text{--}0.591 \text{ \AA}$  in **5–8** (expected  $0.615 \text{ \AA}$ ),<sup>[22]</sup> which demonstrates negligible variations of the  $CrN_6$  chromophores when lanthanides of different sizes occupy the adjacent  $LnN_6O_3$  site. Moreover, the trend  $R_{Nd}^{CN=9} = 1.143 \text{ \AA}$  (expected  $1.163 \text{ \AA}$ )  $>$   $R_{Eu}^{CN=9} = 1.106 \text{ \AA}$  (ex-

Table 1. Selected bond lengths [Å] and angles [°] for [CrNdL<sub>3</sub>](CF<sub>3</sub>SO<sub>3</sub>)<sub>6</sub>(CH<sub>3</sub>CN)<sub>4</sub>(H<sub>2</sub>O) (**5**) and [CrYbL<sub>3</sub>](CF<sub>3</sub>SO<sub>3</sub>)<sub>6</sub>(CH<sub>3</sub>CN)<sub>4</sub> (**7**).

	ligand a		Distances ligand b		ligand c	
	<b>5</b>	<b>7</b>	<b>5</b>	<b>7</b>	<b>5</b>	<b>7</b>
Ln...Cr	9.282(1)	9.334(1)				
Ln-O1	2.456(4)	2.360(4)	2.441(4)	2.310(4)	2.404(4)	2.324(4)
Ln-N4	2.632(5)	2.528(5)	2.628(5)	2.500(5)	2.602(5)	2.513(4)
Ln-N6	2.640(5)	2.515(5)	2.636(5)	2.527(4)	2.658(5)	2.550(5)
Cr-N1	2.075(4)	2.067(5)	2.068(4)	2.074(5)	2.076(5)	2.074(4)
Cr-N2	2.013(5)	2.012(4)	2.022(5)	2.017(4)	2.018(5)	2.027(5)
	ligand a		Angles ligand b		ligand c	
			bite angles			
	<b>5</b>	<b>7</b>	<b>5</b>	<b>7</b>	<b>5</b>	<b>7</b>
N1-Cr-N2	79.5(2)	79.4(2)	79.3(2)	79.3(2)	79.2(2)	79.1(2)
N4-Ln-N6	61.2(1)	63.7(1)	61.8(1)	64.4(1)	62.3(1)	64.4(1)
N6-Ln-O1	62.5(1)	64.6(1)	63.1(1)	64.7(1)	62.6(1)	64.5(1)
N4-Ln-O1	123.5(1)	128.2(1)	124.9(1)	129.0(1)	124.8(1)	128.9(1)
			N-Cr-N			
	<b>5</b>	<b>7</b>			<b>5</b>	<b>7</b>
N1a-Cr-N2b	88.7(2)	89.4(2)	N1a-Cr-N1c		95.7(2)	95.6(2)
N1a-Cr-N2c	174.3(2)	174.2(2)	N2a-Cr-N1b		170.6(2)	171.1(2)
N2a-Cr-N2b	96.9(2)	97.5(2)	N2a-Cr-N1c		88.2(2)	87.9(2)
N2a-Cr-N2c	97.9(2)	97.9(2)	N1a-Cr-N1b		91.9(2)	92.2(2)
N1b-Cr-N1c	96.3(2)	95.9(2)	N1b-Cr-N2c		91.0(2)	90.7(2)
N2b-Cr-N1c	173.9(2)	173.3(2)	N2b-Cr-N2c		96.6(2)	96.1(2)
			N-Ln-N			
	<b>5</b>	<b>7</b>			<b>5</b>	<b>7</b>
N4a-Ln-N4b	87.2(1)	85.1(2)	N6a-Ln-N6b		122.4(1)	121.6(1)
N4b-Ln-N4c	86.0(1)	85.0(1)	N6b-Ln-N6c		118.3(1)	118.8(2)
N4a-Ln-N4c	88.8(1)	87.4(1)	N6a-Ln-N6c		118.5(1)	118.4(1)
N4a-Ln-N6c	147.5(1)	147.1(1)	N4a-Ln-N6b		76.3(1)	74.8(1)
N6a-Ln-N4b	142.3(1)	141.9(1)	N4b-Ln-N6c		76.8(1)	76.3(1)
N6b-Ln-N4c	144.7(1)	145.3(1)	N6a-Ln-N4c		74.1(1)	73.0(1)
			O-Ln-N			
	<b>5</b>	<b>7</b>			<b>5</b>	<b>7</b>
N4a-Ln-O1c	144.2(1)	140.8(1)	N4a-Ln-O1b		77.4(1)	79.5(1)
N6a-Ln-O1b	70.7(1)	68.8(1)	N6a-Ln-O1c		133.9(1)	133.7(1)
N6b-Ln-O1c	68.9(1)	66.6(1)	N4b-Ln-O1c		83.7(1)	84.3(1)
O1a-Ln-N6b	134.5(1)	133.0(1)	O1a-Ln-N4b		145.7(1)	142.9(1)
O1a-Ln-N4c	80.3(1)	81.3(1)	O1a-Ln-N6c		69.0(1)	66.7(1)
O1b-Ln-N4c	144.7(1)	141.6(1)	O1b-Ln-N6c		134.8(1)	133.1(1)
			O-Ln-O			
	<b>5</b>	<b>7</b>			<b>5</b>	<b>7</b>
O1a-Ln-O1b	80.6(1)	79.0(1)	O1b-Ln-O1c		79.6(1)	78.4(1)
O1a-Ln-O1c	78.8(1)	78.1(1)				

pected 1.120 Å) >  $R_{Yb}^{CN=9} = 1.035$  Å (expected 1.042 Å) >  $R_{Lu}^{CN=9} = 1.030$  Å (expected 1.032 Å) calculated with  $r(O) = 1.35$  Å,<sup>[22]</sup> demonstrates the fine tuning provided by the helical strands wrapped around the lanthanide ions. The detailed geometrical analysis of the pseudo-octahedral CrN<sub>6</sub> site based on the angle  $\phi$ ,  $\theta_i$ , and  $\omega_i$  in  $HHH-[CrLnL_3]^{6+}$  (Figure 4a),<sup>[17,23]</sup> shows the usual distortions from a perfect octahedron ( $\phi_{oct} = 180^\circ$ ,  $\theta_{oct} = 54.7^\circ$  and  $\omega_{oct} = 60^\circ$ ) with 1) a faint deviation from the C<sub>3</sub> axis ( $\phi = 178$ – $179^\circ$ , see Table S4 in the Supporting Information), 2) a significant flattening along this axis ( $\theta_i = 57$ – $61^\circ$ , see Table S4 in the Supporting Information), and 3) a constrained helical twist ( $\omega_i = 51$ – $53^\circ$ , see Table S4 in the Supporting Information). As expected, we find identical angular parameters within experimental errors for the four CrN<sub>6</sub> sites in **5**–**8**. A related analysis of

the pseudo-tricapped trigonal prismatic LnN<sub>6</sub>O<sub>3</sub> site in **5**–**8** (Figure 4b),<sup>[17,24]</sup> displays minor variations of  $\phi$  and  $\theta_i$  along the lanthanide series. However,  $\omega_i$  systematically decreases when going from CrNd ( $\omega_i = 14^\circ$ ) to CrLu ( $\omega_i = 9^\circ$ , see Table S5 in the Supporting Information), which indicates a tighter wrapping of the tridentate segments around the smaller lanthanides. This minor structural change is responsible for the systematic increase of the intramolecular Cr...Ln separation with the decreasing size of Ln<sup>III</sup> (Table 2).

This counter-intuitive consequence can be traced back to the mechanical coupling between the adjacent helical portions  $F_{23}$  and  $F_{34}$  defined in Figure 4c.<sup>[17]</sup> The associated helical pitches  $P_{ij}$  (Table 2) unambiguously demonstrate that the tighter wrapping measured by the systematic decrease of  $P_{34}$  and  $P_{45}$  for smaller Ln<sup>III</sup> is balanced by an opposite relaxation of the helical twist within the intermetallic region ( $P_{23}$ ), which eventually dominates the total extension of the helix, as previously reported for  $HHH-[CoLnL_3]^{6+}$  (Ln = La, Lu).<sup>[25]</sup>

**Crystal and molecular structures of  $HHH-[RuEuL_3]-(CF_3SO_3)_5(CH_3OH)_{1.5}(H_2O)$  (**9**) and  $HHH-[RuLuL_3]-(CF_3SO_3)_{4.5}Cl_{0.5}(CH_3OH)_{2.5}$  (**10**):** Compounds **9** and **10**<sup>[19]</sup> are iso-

structural and **9** thus comprises discrete triple-helical cations  $HHH-[RuEuL_3]^{5+}$ , along with ionic triflates and non-coordinated solvent molecules. The numbering used for CrLn also holds for the RuLn series (Figure 3a, and Figure S2 in the Supporting Information). The molecular structures of RuEu and RuLu are almost identical (see Figure S3 in the Supporting Information), while they are only roughly superimposable with the one of CrEu (Figure 5). Selected geometrical parameters are collected in Table 3 and Tables S6–S8 in the Supporting Information.

The calculated ionic radii for Ru<sup>II</sup> in RuEu ( $R_{Ru}^{CN=6} = 0.598$  Å) and RuLu ( $R_{Ru}^{CN=6} = 0.595$  Å)<sup>[19]</sup> point to a negligible influence of the lanthanide contraction onto the pseudo-octahedral RuN<sub>6</sub> chromophore, which is confirmed by identi-

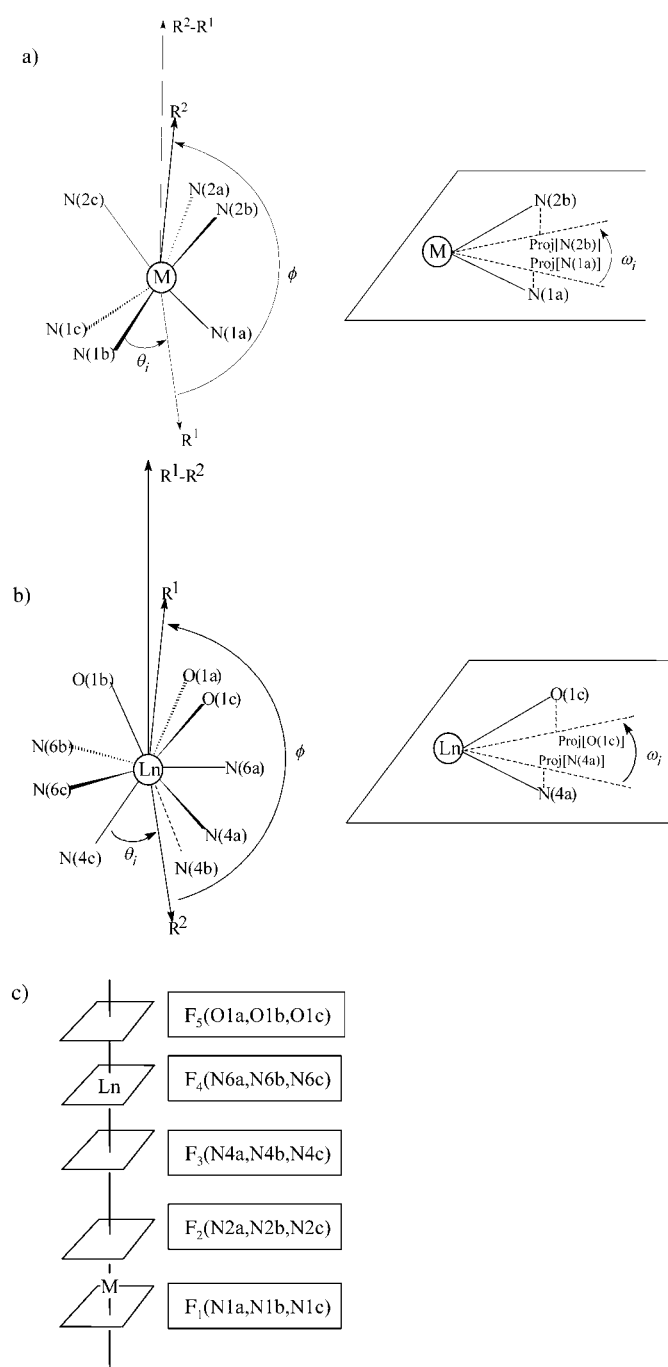


Figure 4. Definition of the angles  $\phi$ ,  $\theta_i$ , and  $\omega_i$  for a) the pseudo-octahedral site ( $R^1 = M-N1a + M-N1b + M-N1c$  and  $R^2 = M-N2a + M-N2b + M-N2c$ )<sup>[23]</sup> and b) the pseudo-tricapped trigonal prismatic site ( $R^1 = Ln-O1a + Ln-O1b + Ln-O1c$  and  $R^2 = Ln-N4a + Ln-N4b + Ln-N4c$ )<sup>[24]</sup> in  $HHH-[MLnL_3]^{6/5+}$  (Proj[N(*i*)] is the projection of N(*i*) along the  $R^1$ - $R^2$  direction onto a perpendicular plane passing through the metal). c) Helical portions  $F_i$  along the threefold axis defined by the facial planes  $F_i$  (see Table S2 and S3 in the Supporting Information).

cal  $\phi$ ,  $\theta_i$ , and  $\omega_i$  angles (see Table S7 in the Supporting Information). Conversely, the contraction of about 0.01 Å observed when replacing Ru<sup>II</sup> with Cr<sup>III</sup> has no significant effect on the wrapping process of the tridentate binding

units around the Ln<sup>III</sup> ions (see Tables S5 and S8 in the Supporting Information). However, the helical twist (measured by  $P_{ij}$ , Figure 4c) shows a global tighter wrapping in going from CrLn to RuLn, which eventually reduces the intermetallic distance by about 0.25 Å (Table 2). Since the geometries of the metallic coordination spheres in CrLn and RuLn are similar, this latter effect is assigned to the larger intermetallic electrostatic repulsion induced by the replacement of Ru<sup>II</sup> with Cr<sup>III</sup>.

**Photophysical properties of the heterobimetallic complexes [CrLnL<sub>3</sub>]<sup>6+</sup> (Ln=Nd, Gd, Yb) and [RuLnL<sub>3</sub>]<sup>5+</sup> (Ln=Nd, Gd, Er, Yb):** According to our structural analysis of complexes 5–10, we can safely conclude that the triple-stranded helicates offer a semi-rigid frame, in which the intermetallic separation is tuned by 1) the electrostatic repulsion between the metal ions and 2) the contraction of the lanthanide ionic radii. This situation is ideal for unravelling the intramolecular intermetallic  $nd \rightarrow 4f$  energy transfer processes eventually leading to the directional conversion of visible light into NIR luminescence. Moreover, the kinetically inert Cr<sup>III</sup>N<sub>6</sub> and Ru<sup>II</sup>N<sub>6</sub> chromophores ensure that the solid state structures are maintained in polar solvents. This is supported by ESI-MS spectra, in which we exclusively detect the presence of  $[MLnL_3]^{6/5+}$  species for sprayed millimolar acetonitrile solutions (see Table S9 in the Supporting Information),<sup>[17,18]</sup> and by the <sup>1</sup>H NMR spectra of  $[RuLnL_3]^{5+}$  (Ln=Nd, Eu, Yb; Table S10 in the Supporting Information), which provide paramagnetic shifts identical to those reported for the analogous C<sub>3</sub>-symmetric triple-helical complexes  $[CoLnL_3]^{6+}$ .<sup>[25]</sup> Direct comparisons between quantum yields measured in solution and excited states lifetimes collected in the solid state are thus reliable.<sup>[17,19,26]</sup>

**Ligand-centered excited states in [CrLnL<sub>3</sub>]<sup>6+</sup> (Ln=Nd, Gd, Yb) and [RuLnL<sub>3</sub>]<sup>5+</sup> (Ln=Nd, Gd, Er, Yb):** The UV part of the absorption spectra of CrLn and RuLn in acetonitrile are similar and show two intense bands centered at 40000 and 30000 cm<sup>-1</sup>, and assigned to ligand-centered  $\pi \rightarrow \pi^*$  transitions, as previously established for CrLu<sup>[17]</sup> and RuLu<sup>[19]</sup> (Table 4, Figure 6a). Excitation of the <sup>1</sup> $\pi\pi^*$  level in CrLn (Ln=Nd, Yb,  $\tilde{\nu}_{exc} = 28170$  and 31545 cm<sup>-1</sup>, respectively) do not produce significant ligand-centered luminescence (10–295 K) because of efficient quenching by Ligand→Cr<sup>III</sup> energy transfer processes, as similarly reported for CrLn (Eu, Gd, Tb, Lu).<sup>[17]</sup> The emission spectra of CrLn are thus dominated by the Cr<sup>III</sup>- and Ln<sup>III</sup>-centered luminescence (vide infra). Similar experiments performed with RuLn (Ln=Nd, Gd, Er, Yb, 77 K) show two bands in the fluorescence spectra around 26100 cm<sup>-1</sup> (ligand-centered <sup>1</sup> $\pi\pi^*$ ) and 17000 cm<sup>-1</sup> (<sup>3</sup>MLCT, Table 4 and Figure 6b), which are diagnostic of the  $[Ru(\alpha, \alpha\text{-diimine})_3]$  chromophore.<sup>[19]</sup> The associated time-resolved spectra (delay time: 50 μs) indicate a weak underlying ligand-centered <sup>3</sup> $\pi\pi^*$  emission (0 phonon: 24300–25000 cm<sup>-1</sup>, lifetimes 70–90 ms, Table 4 and Figure 6b), which points to a somewhat incomplete Ligand→Ru<sup>II</sup> energy transfer process.

Table 2. Helical pitches  $P_{ij}$  along the pseudo- $C_3$  axis<sup>[a]</sup> and intermetallic distances  $d_{M,Ln}$  in the crystal structures of  $[\text{CrLnL}_3](\text{CF}_3\text{SO}_3)_6$  (**5–8**) and  $[\text{RuLnL}_3](\text{CF}_3\text{SO}_3)_5$  (**9, 10**).

	CrNd $P_{ij}$ [Å]	CrEu <sup>[b]</sup> $P_{ij}$ [Å]	CrYb $P_{ij}$ [Å]	CrLu <sup>[b]</sup> $P_{ij}$ [Å]	RuEu $P_{ij}$ [Å]	RuLu <sup>[c]</sup> $P_{ij}$ [Å]
$F_1-F_2$ <sup>[d]</sup>	14.58	14.64	14.58	14.59	13.27	13.35
$F_2-F_3$	20.50	20.63	20.74	20.79	19.83	19.86
$F_3-F_4$	12.40	12.09	11.62	11.61	12.15	12.06
$F_4-F_5$	9.79	9.51	8.90	8.89	8.30	8.72
$F_1-F_5$	15.75	15.67	15.42	15.44	14.83	14.88
$d_{M,Ln}$ [Å]	9.282(1)	9.3238(8)	9.334(1)	9.3546(9)	9.062(1)	9.0794(9)

[a] Each helical portion  $F_1-F_2$ ,  $F_2-F_3$ ,  $F_3-F_4$ , and  $F_4-F_5$  is characterized by 1) a linear extension  $d(F_i-F_j)$  defined by the separation between the facial planes, 2) an average twist angle  $\alpha_{ij}$  defined by the angular rotation between the projections of  $N_i$  and  $N_j$  (or  $O_j$ ) belonging to the same ligand strand onto an intermediate plane passing through the metal (or a midpoint  $X$  for  $F_{25}$ ), and 3) its pitch  $P_{ij}$  defined as the ratio of axial over angular progressions along the helical axis  $P_{ij} = d(F_i-F_j)/(\alpha_{ij}/360)$  ( $P_{ij}$  corresponds to the length of a cylinder containing a single turn of the helix defined by geometrical characteristics  $d(F_i-F_j)$  and  $\alpha_{ij}$ ).<sup>[36]</sup> [b] Taken from ref. [17]. [c] Taken from ref. [19]. [d]  $F_1$ : N1a, N1b, N1c;  $F_2$ : N2a, N2b, N2c;  $F_3$ : N4a, N4b, N4c;  $F_4$ : N6a, N6b, N6c;  $F_5$ : O1a, O1b, O1c (see Figure 4c).

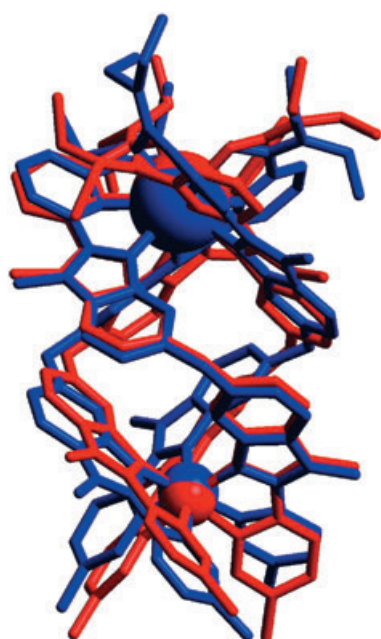


Figure 5. Optimized superimposition of the cations  $HHH-[\text{CrEuL}_3]^{6+}$  (red) and  $HHH-[\text{RuEuL}_3]^{5+}$  (blue) in the structures of **6** and **9**.

**d-Block-centered excited states in  $[\text{CrLnL}_3]^{6+}$  ( $\text{Ln}=\text{Nd, Gd, Yb}$ ) and  $[\text{RuLnL}_3]^{5+}$  ( $\text{Ln}=\text{Nd, Gd, Er, Yb}$ ):** The absorption spectra in the visible range differ for the two series of complexes because the spin-allowed d–d transitions and charge-transfer bands appear at higher energy for  $\text{Cr}^{\text{III}}$  ( ${}^4\text{A}_2 \rightarrow {}^4\text{T}_2$ ,  ${}^4\text{T}_1 + \text{CT}$  in the range  $20\,000\text{--}25\,000\text{ cm}^{-1}$ ),<sup>[17]</sup> than for  $\text{Ru}^{\text{II}}$  ( ${}^1\text{A}_1 \rightarrow {}^1\text{T}_1 + {}^1\text{MLCT}$  in the range  $17\,000\text{--}24\,000\text{ cm}^{-1}$ , Table 4 and Figure 6a).<sup>[19]</sup> At 10 K, in the solid state or in frozen acetonitrile solution, the luminescence spectra of  $\text{CrLn}$  ( $\text{Ln}=\text{Nd, Yb}$ ) display a strong band at  $13\,320\text{ cm}^{-1}$  and Stokes phonon sidebands ( $13\,100\text{--}12\,900\text{ cm}^{-1}$ ) arising from the  $\text{Cr}({}^2\text{E} \rightarrow {}^4\text{A}_2)$  transition, whatever the excitation mode is, through the ligand-centered  ${}^1\pi\pi^*$  level ( $\tilde{\nu}_{\text{exc}} = 29\,170\text{ cm}^{-1}$ ), or upon laser excitation into the Cr-centered bands ( $\tilde{\nu}_{\text{exc}} = 20\,492\text{ cm}^{-1}$ , Figure 7a). At 295 K, the  $\text{Cr}({}^2\text{E})$

luminescence becomes less intense, with the appearance of anti-Stokes side bands ( $13\,700\text{--}14\,200\text{ cm}^{-1}$  Figure 7a).

The associated  $\text{Cr}({}^2\text{E})$  lifetimes in  $\text{CrLn}$  ( $\text{Ln}=\text{Nd, Yb}$ ; Table 4 and Table S11 in the Supporting Information), remain in the millisecond range at 10 K, but are significantly shorter than those obtained for  $\text{CrGd}$  under the same experimental conditions. Since  $\text{Gd}^{\text{III}}$  does not possess accessible excited states below  $32\,200\text{ cm}^{-1}$ ,<sup>[27]</sup> the reduced  $\text{Cr}({}^2\text{E})$  lifetimes in the isostructural complexes  $\text{CrLn}$  ( $\text{Ln}=\text{Nd, Yb}$ ) can be safely assigned to the occurrence of incomplete intramolecular intermetallic  $\text{Cr} \rightarrow \text{Ln}$  energy transfer processes.

At 295 K, the  $\text{Cr}({}^2\text{E})$  lifetimes dramatically decrease to reach the microsecond range as a result of efficient thermally-activated non-radiative vibrational quenching, previously evidenced in  $\text{CrLu}$  and  $\text{CrGd}$  (see Table S11 in the Supporting Information).<sup>[17]</sup> However, the decrease of the Cr-centered emission lifetimes in going from  $\text{CrGd}$  to  $\text{CrLn}$  ( $\text{Ln}=\text{Nd, Yb}$ ) is maintained at 295 K (see Table S11 in the Supporting Information), and further confirmed by a similar trend in the quantum yields  $\Phi_{\text{Cr}}$  measured in acetonitrile (see Table S12 in the Supporting Information). We conclude that partial intramolecular directional intermetallic  $\text{Cr} \rightarrow \text{Ln}$  energy transfer processes also occur at room temperature.

The luminescence spectra of the  $\text{RuLn}$  complexes ( $\text{Ln}=\text{Nd, Gd, Er, Yb}$ ) show a broad band centered around  $15\,000\text{--}17\,000\text{ cm}^{-1}$  (Table 4; 0 phonon at  $15\,600\text{ cm}^{-1}$  at 10 K in the solid state, Figure 8a) arising from the  $\text{Ru}({}^3\text{MLCT})$  state whatever the excitation mode is, through the ligand-centered  ${}^1\pi\pi^*$  level ( $\tilde{\nu}_{\text{exc}} = 31\,145\text{ cm}^{-1}$ ), or upon laser excitation of the  $\text{Ru}({}^1\text{MLCT})$  state ( $\tilde{\nu}_{\text{exc}} = 20\,492\text{ cm}^{-1}$ , Figure 8a). The microsecond  $\text{Ru}({}^3\text{MLCT})$  lifetime is also reduced when going from  $\text{RuGd}$  to the isostructural  $\text{RuLn}$  ( $\text{Ln}=\text{Nd, Er, Yb}$ ) complexes (see Table S11 in the Supporting Information), in complete agreement with the occurrence of partial intermetallic  $\text{Ru} \rightarrow \text{Ln}$  energy transfer processes. Again, this trend is maintained in frozen solution at 10 K (Table 4). However,  $\tau_{\text{Ru}}$  decreases by almost two orders of magnitude at room temperature, and reliable variations of lifetimes in the nanosecond range are difficult to detect with our setup. The concomitant determination of the Ru-centered quantum yields  $\Phi_{\text{Ru}}$  overcomes this limitation, and confirms the existence of intramolecular  $\text{Ru} \rightarrow \text{Ln}$  energy transfers at 295 K (see Table S12 in the Supporting Information).

**f-Block-centered excited states in  $[\text{CrLnL}_3]^{6+}$  ( $\text{Ln}=\text{Nd, Gd, Yb}$ ) and  $[\text{RuLnL}_3]^{5+}$  ( $\text{Ln}=\text{Nd, Gd, Er, Yb}$ ):** The intramolecular d  $\rightarrow$  f energy transfer evidenced in  $\text{CrLn}$  and  $\text{RuLn}$  is re-

Table 3. Selected bond lengths [Å] and angles [°] for [RuEuL<sub>3</sub>](CF<sub>3</sub>SO<sub>3</sub>)<sub>5</sub>(CH<sub>3</sub>OH)<sub>1.5</sub>(H<sub>2</sub>O) (**9**) and [RuLuL<sub>3</sub>](CF<sub>3</sub>SO<sub>3</sub>)<sub>4.5</sub>Cl<sub>0.5</sub>(CH<sub>3</sub>OH)<sub>2.5</sub> (**10**).<sup>[19]</sup>

	ligand a		Distances ligand b		ligand c	
	<b>9</b>	<b>10</b>	<b>9</b>	<b>10</b>	<b>9</b>	<b>10</b>
Ln...Ru	9.062(1)	9.0794(9)				
Ln-O1	2.417(7)	2.345(5)	2.379(7)	2.284(5)	2.405(7)	2.326(4)
Ln-N4	2.621(8)	2.534(6)	2.545(9)	2.469(6)	2.591(8)	2.514(5)
Ln-N6	2.592(7)	2.518(4)	2.623(7)	2.531(5)	2.576(6)	2.515(4)
Ru-N1	2.052(9)	2.064(6)	2.076(6)	2.060(5)	2.059(7)	2.055(5)
Ru-N2	2.058(7)	2.051(5)	2.042(8)	2.044(5)	2.059(6)	2.057(5)
	ligand a		Angles ligand b		ligand c	
	<b>9</b>	<b>10</b>	<b>9</b>	<b>10</b>	<b>9</b>	<b>10</b>
			bite angles			
N1-Ru-N2	77.5(4)	77.8(2)	77.2(3)	77.5(2)	77.5(3)	77.9(2)
N4-Ln-N6	62.9(2)	64.5(2)	62.7(3)	64.5(2)	63.6(3)	64.7(2)
N6-Ln-O1	62.4(2)	63.8(2)	63.0(2)	64.2(2)	64.2(2)	65.2(2)
N4-Ln-O1	125.1(2)	128.2(1)	125.7(2)	128.7(2)	127.5(2)	129.6(2)
			N-Ru-N			
	<b>9</b>	<b>10</b>			<b>9</b>	<b>10</b>
N1a-Ru-N2b	175.7(2)	175.7(2)	N1a-Ru-N1c		95.8(3)	95.0(2)
N1a-Ru-N2c	84.9(3)	85.0(2)	N2a-Ru-N1b		85.2(3)	85.5(2)
N2a-Ru-N2b	100.3(3)	99.8(2)	N2a-Ru-N1c		172.8(3)	172.5(2)
N2a-Ru-N2c	99.1(3)	99.3(2)	N1a-Ru-N1b		98.9(3)	98.7(2)
N1b-Ru-N1c	98.6(3)	97.7(2)	N1b-Ru-N2c		174.9(3)	174.5(2)
N2b-Ru-N1c	86.6(3)	87.5(2)	N2b-Ru-N2c		99.1(3)	99.0(2)
			N-Ln-N			
	<b>9</b>	<b>10</b>			<b>9</b>	<b>10</b>
N4a-Ln-N4b	89.1(3)	88.3(2)	N6a-Ln-N6b		119.3(2)	119.5(2)
N4b-Ln-N4c	82.9(2)	82.7(2)	N6b-Ln-N6c		117.4(2)	117.4(2)
N4a-Ln-N4c	84.4(2)	83.9(2)	N6a-Ln-N6c		121.7(2)	121.5(2)
N4a-Ln-N6c	76.3(2)	74.7(2)	N4a-Ln-N6b		148.0(3)	148.0(2)
N6a-Ln-N4b	77.0(2)	75.6(2)	N4b-Ln-N6c		144.2(2)	144.3(2)
N6b-Ln-N4c	77.8(2)	76.5(2)	N6a-Ln-N4c		141.4(3)	141.6(2)
			O-Ln-N			
	<b>9</b>	<b>10</b>			<b>9</b>	<b>10</b>
N4a-Ln-O1c	78.8(3)	79.1(2)	N4a-Ln-O1b		141.7(2)	139.9(2)
N6a-Ln-O1b	133.7(2)	132.1(2)	N6a-Ln-O1c		68.3(2)	67.4(2)
N6b-Ln-O1c	132.9(3)	132.7(2)	N4b-Ln-O1c		145.1(2)	142.8(1)
O1a-Ln-N6b	68.6(2)	67.5(2)	O1a-Ln-N4b		82.3(3)	82.7(2)
O1a-Ln-N4c	146.5(2)	144.1(2)	O1a-Ln-N6c		132.8(3)	132.4(2)
O1b-Ln-N4c	84.7(2)	86.1(2)	O1b-Ln-N6c		66.0(2)	65.9(2)
			O-Ln-O			
	<b>9</b>	<b>10</b>			<b>9</b>	<b>10</b>
O1a-Ln-O1b	79.9(2)	77.9(2)	O1b-Ln-O1c		79.1(2)	77.9(2)
O1a-Ln-O1c	78.5(2)	78.3(2)				

responsible for the concomitant Ln-centered NIR emission detected in the 7150–11800 cm<sup>-1</sup> range for the Nd(<sup>4</sup>F<sub>3/2</sub>→<sup>4</sup>I<sub>J</sub>; J=9/2, 11/2, 13/2) transitions (Figure 7b–d and Figure S4 in the Supporting Information), 9200–10800 cm<sup>-1</sup> range for the Yb(<sup>2</sup>F<sub>5/2</sub>→<sup>2</sup>F<sub>7/2</sub>) transition (Figure 8b and Figure S5 in the Supporting Information), and 6500–6600 cm<sup>-1</sup> range for the Er(<sup>4</sup>I<sub>13/2</sub>→<sup>4</sup>I<sub>15/2</sub>) transition (see Figure S6 in the Supporting Information). Since the local environments of the pseudo-tricapped trigonal-prismatic LnN<sub>6</sub>O<sub>3</sub> sites are comparable in CrLn and RuLn (see crystallographic section), the crystal-field splitting of the Nd- and Yb-centered transitions are almost identical (see Table S13 in the Supporting Information). It can be interpreted as arising from metal ions in a trigonal site with D<sub>3</sub> symmetry, for which the irreducible representations of the total angular momentum operator

lead to four sublevels for Yb(<sup>2</sup>F<sub>7/2</sub>) and three sublevels for Yb(<sup>2</sup>F<sub>5/2</sub>) (Figure 9a).<sup>[28]</sup> We thus expect four transitions from the lowest crystal-field sublevel of Yb(<sup>2</sup>F<sub>5/2</sub>) to the Yb(<sup>2</sup>F<sub>7/2</sub>) manifold (Figure 8b, and Figure S5 and Table S13 in the Supporting Information). At 10 K, the total splitting of Yb(<sup>2</sup>F<sub>7/2</sub>) amounts to 304 cm<sup>-1</sup> in CrYb and 303 cm<sup>-1</sup> in RuYb, which confirms the similarity of the lanthanide coordination spheres in these helicates. The Nd(<sup>4</sup>F<sub>3/2</sub>)-centered luminescence in CrNd (Figure 7b–d) and RuNd (see Figure S4 in the Supporting Information) features the typical three transitions to <sup>4</sup>I<sub>J</sub> (J=9/2, 11/2, 13/2) split into five (<sup>4</sup>I<sub>9/2</sub>, 10800–11600 cm<sup>-1</sup>), five (<sup>4</sup>I<sub>11/2</sub>, 9200–9500 cm<sup>-1</sup>), and seven components (<sup>4</sup>I<sub>13/2</sub>, 7150–7700 cm<sup>-1</sup>), for which we predict respectively, five, six, and seven allowed transitions assuming a trigonal symmetry.<sup>[16]</sup> Upon increasing the temperature, the <sup>4</sup>F<sub>3/2</sub>-centered emission band becomes broader, the energy difference between the components within each <sup>4</sup>I<sub>J</sub> manifold remaining the same (see Table S13 in the Supporting Information). However, additional components, shifted by 65–75 cm<sup>-1</sup> on the high energy sides of the initial transitions (Figure 7b–d, and Figure S4 and Table S13 in the Supporting Information), can be assigned as originating from the highest crystal-field sublevel of the emitting <sup>4</sup>F<sub>3/2</sub> excited state (Figure 9b). Using a Boltzmann distribution with T=295 K and ΔE=70 cm<sup>-1</sup>, we calculate a 41% population for the upper sublevel, in line with the intensity ratios of the 11509 cm<sup>-1</sup>/11436 cm<sup>-1</sup> components of the <sup>4</sup>F<sub>3/2</sub>→<sup>4</sup>I<sub>9/2</sub> transition, which amount to 0.38 for CrNd and 0.43 for RuNd. In the case of RuEr, the poor resolution of the Er(<sup>4</sup>I<sub>13/2</sub>→<sup>4</sup>I<sub>15/2</sub>) transition prevents a detailed crystal-field analysis (see Figure S6 in the Supporting Information).

Interestingly, the Yb(<sup>2</sup>F<sub>5/2</sub>) and Nd(<sup>4</sup>F<sub>3/2</sub>) emission decays at 10 K are single exponential functions, but the corresponding lifetimes cover three orders of magnitude, that is, from millisecond (CrNd, CrYb) to microsecond (RuNd, RuYb) ranges (Table 5). Comparison with the standard Ln-centered

Table 4. Ligand-centered and d-block-centered absorption and emission properties of complexes  $[\text{CrLnL}_3]^{6+}$  (Ln = Nd, Gd, Yb) and  $[\text{RuLnL}_3]^{5+}$  (Ln = Nd, Gd, Er, Yb) in acetonitrile.<sup>[a]</sup>

Compd	Absorption [ $\text{cm}^{-1}$ ] $\pi \rightarrow \pi^*$ <sup>[b]</sup>	Absorption [ $\text{cm}^{-1}$ ] d-d + CT <sup>[b]</sup>	Emission [ $\text{cm}^{-1}$ ] $^1\pi\pi^*$	Emission [ $\text{cm}^{-1}$ ] $^3\pi\pi^*$	Lifetime [ms] $\tau(^3\pi\pi^*)$	Emission [ $\text{cm}^{-1}$ ] d-block-centered	Lifetime [ $\mu\text{s}$ ] <sup>[c]</sup> d-block-centered
CrGd	40486 (78200 sh) 29940 (102200)	25700 (26000 sh) 22800 (2400 sh)	[d]	[d]	[d]	13301 Cr( $^2\text{E}$ )	$4.21(2) \times 10^3$
CrNd	40486 (81700 sh) 29940 (96900)	25700 (21400 sh) 22800 (2700 sh)	[d]	[d]	[d]	13330 Cr( $^2\text{E}$ )	$0.58(3) \times 10^3$
CrYb	40486 (77100 sh) 29940 (96900)	25700 (21300 sh) 22800 (2800 sh)	[d]	[d]	[d]	13327 Cr( $^2\text{E}$ )	$2.53(2) \times 10^3$
RuGd	40160 (79025) 30120 (105900)	21185 (8700)	25800	24300(sh) 20700	94(4)	14493 Ru( $^3\text{MLCT}$ )	12.4(7)
RuNd	40160 (77750) 30120 (111660)	21185 (9400)	26200	25100(sh) 23000	73(3)	14493 Ru( $^3\text{MLCT}$ )	6.27(3)
RuEr	40160 (77080) 30120 (105500)	21185 (8300)	26000	25700(sh) 22600	93(5)	14493 Ru( $^3\text{MLCT}$ )	9.72(4)
RuYb	40160 (78030) 30120 (103300)	21185 (8500)	26200	25600(sh) 23600	94(4)	14493 Ru( $^3\text{MLCT}$ )	9.16(2)

[a] Absorption spectra recorded at 293 K, luminescence data and lifetime measurements at 77 K ( $\bar{\nu}_{\text{exc}} = 31545 \text{ cm}^{-1}$ ); sh = shoulder. [b] Energies are given for the maximum of the band envelope in  $\text{cm}^{-1}$  and  $\epsilon$  (in parentheses) in  $\text{M}^{-1}\text{cm}^{-1}$ . [c] At 10 K. [d]  $^1\pi\pi^*$  and  $^3\pi\pi^*$  luminescence quenched by transfer to  $\text{Cr}^{\text{III}}$  ion.<sup>[17]</sup>

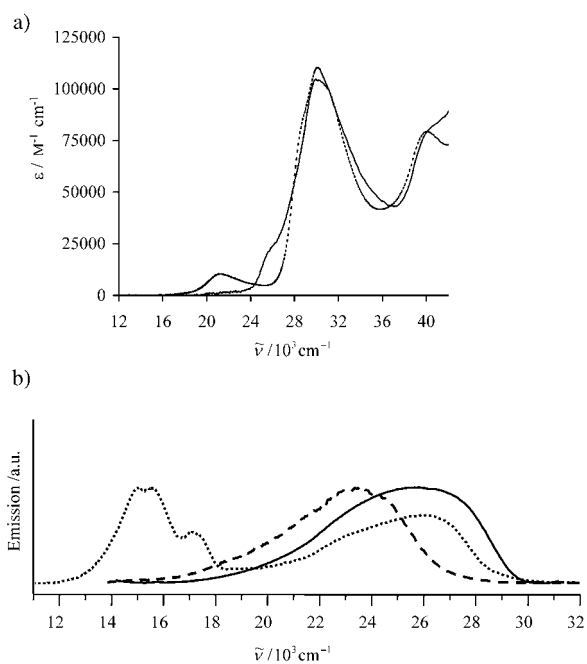


Figure 6. a) Absorption spectra of  $HHH\text{-}[\text{CrNdL}_3]^{6+}$  (full line) and  $HHH\text{-}[\text{RuNdL}_3]^{5+}$  (dashed line) in acetonitrile (293 K,  $10^{-3} \text{ mol dm}^{-3}$ ). b) Emission spectrum of  $HHH\text{-}[\text{RuYbL}_3]^{5+}$  in acetonitrile at 293 K (full line), at 77 K (dotted line), and at 77 K with a 0.05 ms delay time (dashed line,  $10^{-3} \text{ mol dm}^{-3}$ ,  $\bar{\nu}_{\text{exc}} = 31545 \text{ cm}^{-1}$ ).

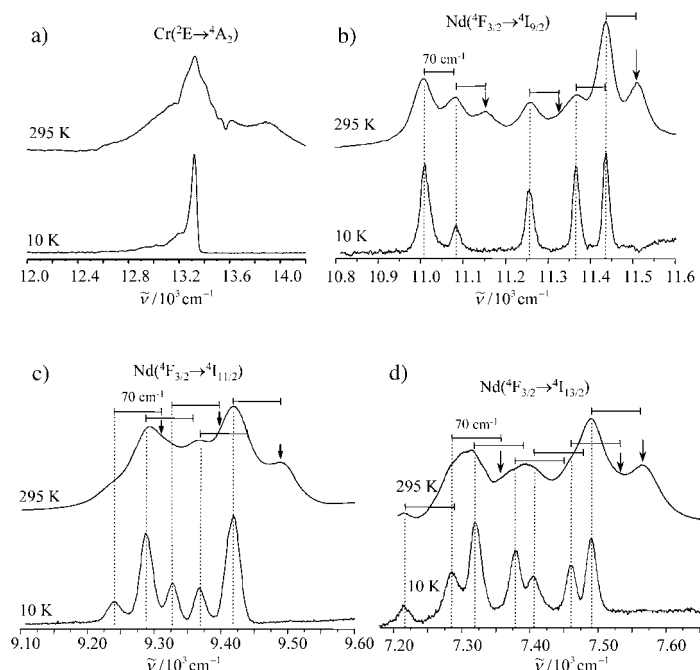


Figure 7. Emission spectra of  $HHH\text{-}[\text{CrNdL}_3]^{6+}$  in the solid state at 10 K and 295 K ( $\bar{\nu}_{\text{exc}} = 20492 \text{ cm}^{-1}$ ). a) Cr( $^2\text{E} \rightarrow ^4\text{A}_2$ ) transition and b)–d) Nd( $^4\text{F}_{3/2} \rightarrow ^4\text{I}_J$ ,  $J = 9/2, 11/2, 13/2$ , respectively) transitions. Arrows point to transition arising from the highest crystal-field sublevel.

luminescence decay times measured in absence of d  $\rightarrow$  f communication in  $HHH\text{-}[\text{ZnNdL}_3]^{5+}$  ( $\tau(^4\text{F}_{3/2}) = 1.4\text{--}1.8 \mu\text{s}$ , Table 5) and in  $HHH\text{-}[\text{ZnYbL}_3]^{5+}$  ( $\tau(^2\text{F}_{5/2}) = 20\text{--}22 \mu\text{s}$ , Table 5) shows that, except for RuYb, the NIR Ln-centered

luminescence decays are significantly slower in the CrLn and RuLn complexes.

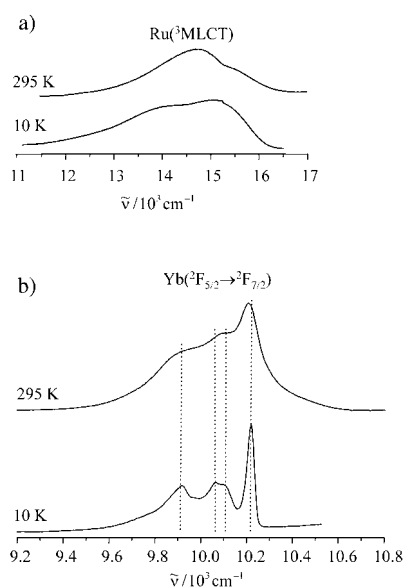


Figure 8. Emission spectra of  $HHH-[RuYbL_3]^{5+}$  in the solid state at 10 K and 295 K ( $\bar{\nu}_{ex} = 20492 \text{ cm}^{-1}$ ). a)  $Ru(^3MLCT)$  transition and b)  $Yb(^2F_{5/2} \rightarrow ^2F_{7/2})$  transition.

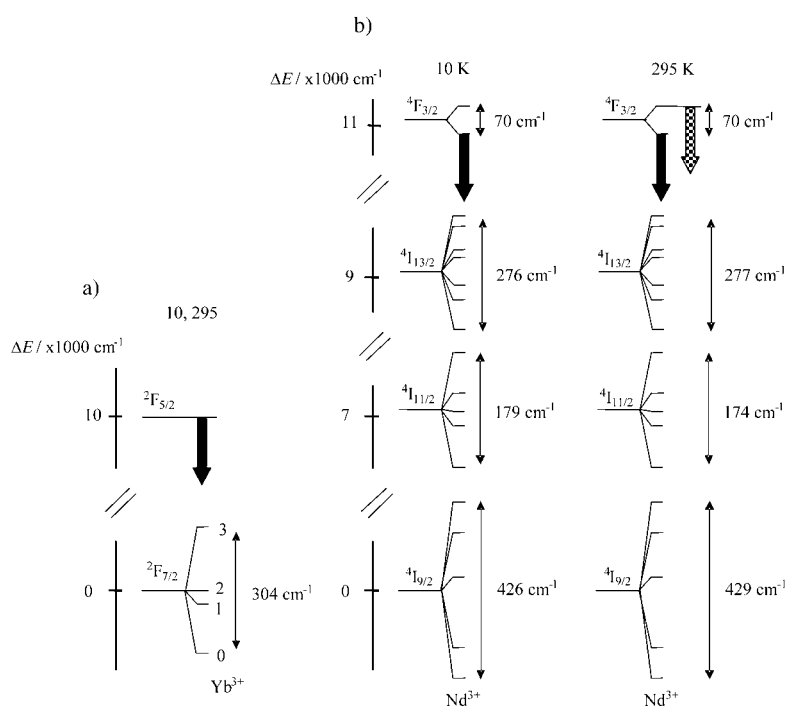


Figure 9. Ligand-field sublevels of a)  $Yb^{III}$  and b)  $Nd^{III}$  as determined from emission spectra at 10 and 295 K in  $HHH-[CrLnL_3]^{6+}$ .

### Models and consequences of intramolecular d→f energy transfers in $[CrLnL_3]^{6+}$ ( $Ln=Nd, Yb$ ) and $[RuLnL_3]^{5+}$ ( $Ln=Nd, Er, Yb$ ):

A close scrutiny of the emission spectra of  $CrNd$  or  $RuNd$  shows several dips in the profile of the  $Cr(^2E)$  and  $Ru(^3MLCT)$  transitions, which exactly match the  $^4I_{9/2} \rightarrow (^4F_{5/2}, ^2H_{9/2})$  absorption of the neighbouring  $Nd^{III}$  ion (Figure 7a, and Figure S7 in the Supporting Information). This is evidence for a  $M \rightarrow Nd$  energy transfer process, which

can be modelled by the simple kinetic scheme given in Figure 10.

The mathematical treatment of this system leads to the rate Equations (3) and (4), which can be integrated to give the time-dependent concentration of the excited species  $[M^*(t)]$  [Eq. (5)] and  $[Ln^*(t)]$  [Eq. (6)], in which  $M$  and  $Ln$  stand for the d- and f-block metal ions, respectively.<sup>[29]</sup>

$$d[M^*(t)]/dt = -(k_{ET}^{M,Ln} + k_{Lum}^M)[M^*(t)] \quad (3)$$

$$d[Ln^*(t)]/dt = k_{ET}^{M,Ln}[M^*(t)] - k_{Lum}^{Ln}[Ln^*(t)] \quad (4)$$

$$[M^*(t)] = [M^*(0)]e^{-(k_{ET}^{M,Ln} + k_{lum}^M)t} = [M^*(0)]e^{-k_{obs}^M t} \quad (5)$$

$$[Ln^*(t)] = [M^*(0)] \frac{k_{ET}^{M,Ln}}{k_{Lum}^{Ln} - (k_{ET}^{M,Ln} + k_{Lum}^M)} (e^{-(k_{ET}^{M,Ln} + k_{Lum}^M)t} - e^{-k_{Lum}^{Ln}t}) \quad (6)$$

The metal-centered luminescence rate constants  $k_{Lum}^M$  and  $k_{Lum}^{Ln}$  correspond to the sum of the radiative and non-radiative de-excitation pathways in absence of the acceptor

( $k_{Lum}^M$ ), or of the donor ( $k_{Lum}^{Ln}$ ).  $k_{Lum}^M$  is thus reasonably approximated by the decay rate constant of the d-block-centered luminescence in  $CrGd$  and  $RuGd$  (Table 4, and Table S11 in the Supporting Information), while  $k_{Lum}^{Ln}$  is obtained from the f-block-centered emission in  $ZnLn$  ( $Ln=Nd, Yb, Er$ , Table 5).<sup>[30]</sup> Assuming that the intramolecular d→f directional energy transfer is the only additional non-radiative pathway affecting the deactivation of the d-block-centered excited state in  $CrLn$  or  $RuLn$ , when  $Nd^{III}$ ,  $Er^{III}$  or  $Yb^{III}$  replace  $Gd^{III}$ , the rate constant of the energy transfer process,  $k_{ET}^{M,Ln}$ , can be estimated from Equation (7), in which  $k_{obs}^M$  is the experimental observed decay rate constant of  $M^*$  in presence of the  $Ln$  acceptor in the  $[MLnL_3]^{5/6+}$  complexes ( $M=Cr, Ru$ ;  $Ln=Nd, Er, Yb$ ; Table 4 and Table S11).<sup>[2b,18]</sup>

$$k_{ET}^{M,Ln} = k_{obs}^M - k_{Lum}^M = (\tau_{obs}^M)^{-1} - (\tau_{Lum}^M)^{-1} \quad (7)$$

Moreover, once  $k_{ET}^{M,Ln}$  is determined, Equation (1) holds, thus leading to the critical distances for 50% energy transfer processes  $R_0^{M,Ln}$  collected in Table 6.

At 10 K, a temperature at which phonon-assisted energy transfer processes are minimized, we notice that 1)  $Cr^{III}$  is a

Table 5. f-Block-centered lifetimes ( $\tau$  [ $\mu\text{s}$ ]) for  $\text{Nd}({}^4\text{F}_{3/2})$ ,  $\text{Yb}({}^2\text{F}_{5/2})$ , and  $\text{Er}({}^4\text{I}_{3/2})$  in  $\text{HHH}[\text{CrLnL}_3]^{6+}$  ( $\text{Ln}=\text{Nd}, \text{Yb}$ ),  $\text{HHH}[\text{RuLnL}_3]^{5+}$  ( $\text{Ln}=\text{Nd}, \text{Er}, \text{Yb}$ ), and  $\text{HHH}[\text{ZnLnL}_3]^{5+}$  ( $\text{Ln}=\text{Nd}, \text{Yb}$ ).

Compd	Solid-state/ 10 K	Solution/ 10 K [a]	Solid-state/ 295 K	Solution/ 295 K [a]
CrNd [b]	$0.47(1) \times 10^3$	$0.54(1) \times 10^3$	$0.12(1) \times 10^3$	5.1(1)
CrYb [b]	$1.96(1) \times 10^3$	$2.45(1) \times 10^3$	$0.24(1) \times 10^3$	23(2)
RuNd [c]	6.04(3)	5.79(7)	1.44(2)	[d]
RuEr [c]	6.94(5)	[d]	0.540(5)	[d]
RuYb [c]	22.72(7)	22.4(1)	17.52(2)	22.6(2)
ZnNd [b]	1.46(1)	1.49(1)	1.60(1)	1.82(1)
ZnYb [b]	20(1)	23(2)	23(1)	22(1)

[a]  $10^{-4} \text{ mol dm}^{-3}$  in acetonitrile. [b]  $\tilde{\nu}_{\text{exc}} = 28169 \text{ cm}^{-1}$ . [c]  $\tilde{\nu}_{\text{exc}} = 20492 \text{ cm}^{-1}$ . [d] Too weak to be measured.

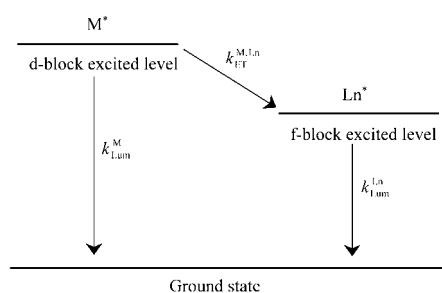


Figure 10. Kinetic model for the deactivation and communication of d-block and f-block-centered excited levels in  $\text{HHH}[\text{MLnL}_3]^{5/6+}$  ( $\text{M}=\text{Cr}, \text{Ru}; \text{Ln}=\text{Nd}, \text{Er}, \text{Yb}$ ).

better donor than  $\text{Ru}^{\text{II}}$  ( $\eta_{\text{ET}}^{\text{Cr, Ln}} > \eta_{\text{ET}}^{\text{Ru, Ln}}$ , Table 6) and 2) the efficiency of the energy transfer process decreases in the order  $\eta_{\text{ET}}^{\text{M, Nd}} > \eta_{\text{ET}}^{\text{M, Er}} > \eta_{\text{ET}}^{\text{M, Yb}}$ . Therefore, larger critical distances are calculated for the CrLn complexes ( $R_0^{\text{Cr, Ln}} > R_0^{\text{Ru, Ln}}$ ), and with  $\text{Ln}=\text{Nd}$  (Table 6). The latter effect can be assigned

to an increase of the overlap integral  $J$  [Eq. (2)] when  $\text{Nd}^{\text{III}}$  is used as an acceptor because its  ${}^4\text{F}_J$  ( $J=3/2, 5/2, 7/2, 9/2$ ),  ${}^2\text{H}_J$  ( $J=9/2, 11/2$ ), and  ${}^4\text{S}_{3/2}$  excited levels are available for overlapping with the M-centered emission spectra in the  $13000\text{--}15000 \text{ cm}^{-1}$  range, while only two ( ${}^4\text{F}_{9/2}$  and  ${}^4\text{I}_{9/2}$ ) and one level ( ${}^2\text{F}_{5/2}$ ) are accessible for  $\text{Ln}=\text{Er}$  and  $\text{Yb}$ , respectively.<sup>[10]</sup> At 295 K, the thermally-activated vibrational processes explain the faster luminescence decays of the donor  $k_{\text{Lum}}^{\text{M}}$ , but the parallel trend observed for the energy transfer process  $k_{\text{ET}}^{\text{M, Ln}}$  suggests that both M-centered de-excitation processes (i.e., luminescence and energy transfer, Table 6) depend on closely related phonon-assisted mechanisms at high temperature. Consequently, the efficiency of the energy transfer processes  $\eta_{\text{ET}}^{\text{M, Ln}} = k_{\text{ET}}^{\text{M, Ln}} / (k_{\text{Lum}}^{\text{M}} + k_{\text{ET}}^{\text{M, Ln}}) = k_{\text{ET}}^{\text{M, Ln}} / k_{\text{obs}}^{\text{M}}$  [Eq. (1)] does not drastically vary with temperature (Table 6). It is worth noting that  $k_{\text{ET}}^{\text{Ru, Nd}} = 2.3 \times 10^6 \text{ s}^{-1}$  and  $k_{\text{ET}}^{\text{Ru, Yb}} = 5.2 \times 10^5 \text{ s}^{-1}$  obtained at 295 K are comparable to rate constants reported for similar processes in the more flexible complexes **1** and **2** (Figure 1). A similar behavior is observed for CrLn and RuLn in acetonitrile solution and the efficiency of the energy transfer process ( $\eta_{\text{ET}}^{\text{M, Ln}}$ , [Eq. (8)]) and critical distance ( $R_0^{\text{M, Ln}}$ , [Eq. (1)]),<sup>[17]</sup> fairly match those obtained in the solid state (see Table S14 in the Supporting Information).

$$\eta_{\text{ET}}^{\text{M, Ln}} = 1 - (\Phi_{\text{M, Ln}} / \Phi_{\text{M, Gd}}) \quad (8)$$

However, the most striking point concerns the experimental apparent rate constants  $k_{\text{App}}^{\text{Ln}}$  of the Ln-centered luminescence in  $[\text{MLnL}_3]^{5/6+}$  ( $\text{Ln}=\text{Nd}, \text{Er}, \text{Yb}$ ), which are orders of magnitude smaller than those found for the intrinsic luminescence ( $k_{\text{Lum}}^{\text{Ln}}$ ) measured in absence of donor in  $[\text{ZnLnL}_3]^{5+}$  (Table 6). In other words, the expected lifetimes of the Ln-centered luminescence, which are in the microsec-

Table 6. Experimental rates of luminescence  $k_{\text{Lum}}^{\text{M}}$ ,  $k_{\text{Lum}}^{\text{Ln}}$ ,  $k_{\text{obs}}^{\text{M}}$ , and  $k_{\text{App}}^{\text{Ln}}$ , and calculated energy transfer rates  $k_{\text{ET}}^{\text{M, Ln}}$  [Eq. (7)], efficiencies  $\eta_{\text{ET}}^{\text{M, Ln}}$ , and critical distances  $R_0^{\text{M, Ln}}$  [Eq. (1)], and switching distances  $d_{\text{switch}}^{\text{M, Ln}}$  [Eq. (11)] for  $\text{HHH}[\text{CrLnL}_3]^{6+}$  ( $\text{Ln}=\text{Nd}, \text{Yb}$ ),  $\text{HHH}[\text{RuLnL}_3]^{5+}$  ( $\text{Ln}=\text{Nd}, \text{Er}, \text{Yb}$ ), and  $\text{HHH}[\text{ZnLnL}_3]^{5+}$  ( $\text{Ln}=\text{Nd}, \text{Yb}$ ) in the solid state.<sup>[a]</sup>

Compd	$T$ [K]	$k_{\text{obs}}^{\text{M}}$ [ $\text{s}^{-1}$ ]	$k_{\text{Lum}}^{\text{M}}$ [ $\text{s}^{-1}$ ]	$k_{\text{App}}^{\text{Ln}}$ [ $\text{s}^{-1}$ ]	$k_{\text{Lum}}^{\text{Ln}}$ [ $\text{s}^{-1}$ ]	$k_{\text{ET}}^{\text{M, Ln}}$ [ $\text{s}^{-1}$ ]	$\eta_{\text{ET}}^{\text{M, Ln}}$ [%]	$R_0^{\text{M, Ln}}$ [Å]	$R_{\text{DA}}^{\text{M, Ln}}$ <sup>[b]</sup> [Å]	$d_{\text{switch}}^{\text{M, Ln}}$ [Å]
ZnNd	10				$6.84 \times 10^5$					
ZnYb	10				$5.00 \times 10^4$					
CrGd	10		$2.73 \times 10^2$							
CrNd	10	$2.13 \times 10^3$		$2.13 \times 10^3$		$1.86 \times 10^3$	87	12.8	9.28	3.5
CrYb	10	$5.10 \times 10^2$		$5.10 \times 10^2$		$2.37 \times 10^2$	46	9.1	9.33	3.8
RuGd	10		$1.04 \times 10^5$							
RuNd	10	$1.55 \times 10^5$		$1.65 \times 10^5$		$5.10 \times 10^4$	33	8.1	9.06	5.9
RuEr	10	$1.44 \times 10^5$		$1.44 \times 10^5$		$4.00 \times 10^4$	28	7.7	9.08	
RuYb	10	$1.27 \times 10^5$		4.404		$2.30 \times 10^4$	18	7.1	9.08	8.0
ZnNd	295				$6.25 \times 10^5$					
ZnYb	295				$4.35 \times 10^4$					
CrGd	295		$3.45 \times 10^3$							
CrNd	295	$8.33 \times 10^3$		$8.33 \times 10^3$		$4.88 \times 10^3$	59	9.8	9.28	4.1
CrYb	295	$4.17 \times 10^3$		$4.17 \times 10^3$		$7.20 \times 10^2$	17	7.2	9.33	4.7
RuGd	295		$1.16 \times 10^6$							
RuNd	295	$3.45 \times 10^6$		$6.94 \times 10^5$		$2.29 \times 10^6$	66	10.2	9.06	11.3
RuEr	295	$1.85 \times 10^6$		$1.85 \times 10^6$		$6.90 \times 10^5$	37	8.4	9.08	
RuYb	295	$1.68 \times 10^6$		$5.71 \times 10^4$		$5.20 \times 10^5$	31	7.9	9.08	13.7

[a] Typical relative error  $\pm 10\%$ . [b] Intermetallic distances taken from the crystal structures of **5–10**.

ond range ( $\tau_{\text{ZnNd}} = (k_{\text{lum}}^{\text{ZnNd}})^{-1} = 1.46 \mu\text{s}$ ,  $\tau_{\text{ZnYb}} = (k_{\text{lum}}^{\text{ZnYb}})^{-1} = 20 \mu\text{s}$ ), can be apparently lengthened by factors  $10^1$ – $10^3$  in RuLn and CrLn, respectively. This known phenomenon<sup>[2b]</sup> depends on the ratio  $r = k_{\text{lum}}^{\text{Ln}} / (k_{\text{lum}}^{\text{M}} + k_{\text{ET}}^{\text{M,Ln}}) = 1 - \eta_{\text{ET}}^{\text{M,Ln}}$ ,<sup>[2b]</sup> and it can be rationalized with Equation (6). A first limiting case occurs when the energy transfer is very fast and consequently, the sum  $k_{\text{obs}}^{\text{M,Ln}} = (k_{\text{lum}}^{\text{M}} + k_{\text{ET}}^{\text{M,Ln}})$  is much larger than  $k_{\text{lum}}^{\text{Ln}}$  ( $r \ll 1$ ); Equation (6) then reduces to Equation (9), in which the apparent decay of the Ln-centered luminescence in the bimetallic complex MLn coincides with the one found in absence of a donor in ZnLn ( $k_{\text{lum}}^{\text{Ln}}$ ).

$$[\text{Ln}^*(t)] = [\text{M}^*(0)] \frac{k_{\text{ET}}^{\text{M,Ln}}}{(k_{\text{ET}}^{\text{M,Ln}} + k_{\text{lum}}^{\text{Ln}})} e^{-k_{\text{lum}}^{\text{Ln}} t} \quad (9)$$

This situation is found for RuYb, for which  $(k_{\text{lum}}^{\text{Ru}} + k_{\text{ET}}^{\text{Ru,Yb}}) = 1.27 \times 10^5 \text{ s}^{-1} \gg k_{\text{lum}}^{\text{Yb}} = 5.0 \times 10^4 \text{ s}^{-1}$  at 10 K (Table 6). Equation (6) predicts that the population of the excited lanthanide level  $\text{Yb}(^2\text{F}_{5/2})$  in RuYb culminates around 5% with respect to  $[\text{Ru}^*(t=0)] = 100\%$  (Figure 11a), and the experimental apparent  $\text{Yb}(^2\text{F}_{5/2})$  decay lifetime ( $\tau = 22.7(1) \mu\text{s}$ , Table 5), indeed fits the one obtained in absence of a donor ( $\tau_{\text{ZnYb}} = 20 \mu\text{s}$ ). The second limiting case is more intriguing and it arises when the sum of the energy transfer and d-block-centered deactivation rates are small in

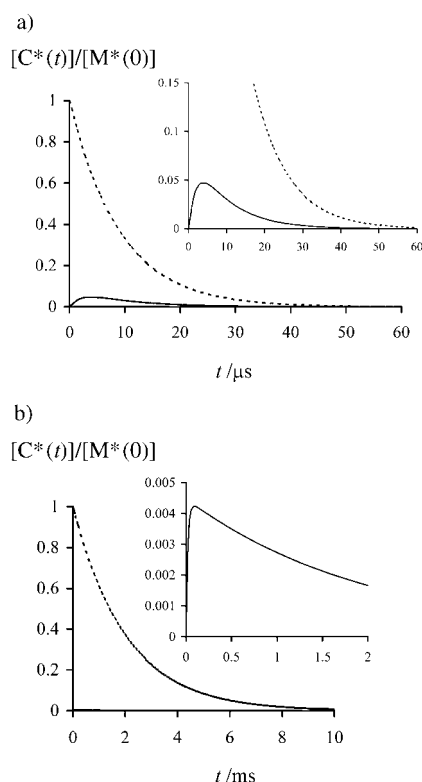


Figure 11. Illustration of the time-dependent concentrations  $[\text{M}^*(t)]$  (dotted lines) and  $[\text{Ln}^*(t)]$  (full lines) for the deactivation of d-block- and f-block-centered excited levels in a)  $\text{HHH}[\text{RuYbL}_3]^{5+}$  and b)  $\text{HHH}[\text{CrYbL}_3]^{6+}$  (solid-state, 10 K). The expansions highlight the two-order magnitude change in the apparent decay of the  $\text{Yb}(^2\text{F}_{5/2})$  level when  $\text{Ru}^{\text{II}}$  or  $\text{Cr}^{\text{III}}$  are used as sensitizers.

comparison with the Ln-centered deactivation:  $(k_{\text{lum}}^{\text{M}} + k_{\text{ET}}^{\text{M,Ln}}) = k_{\text{obs}}^{\text{M}} \ll k_{\text{lum}}^{\text{Ln}}$  ( $r \gg 1$ ). Equation (6) thus transforms into Equation (10), and the decay of the Ln-centered luminescence is now determined by the population rate of the Ln excited level by directional energy transfer from the M ion. It therefore mirrors that of the d-block donor.

$$[\text{Ln}^*(t)] = [\text{M}^*(0)] \frac{k_{\text{ET}}^{\text{M,Ln}}}{k_{\text{lum}}^{\text{Ln}}} e^{-k_{\text{obs}}^{\text{M}} t} \quad (10)$$

The latter situation holds for RuNd, CrNd, and CrYb (Figure 11b, and Figure S8 in the Supporting Information) and leads to an astonishing apparent lengthening of the Ln-centered emission decay time in the millisecond range when  $\text{Cr}^{\text{III}}$  is used as donor.

## Conclusion

Detailed structural investigation of the CrLn (Ln = Nd, Eu, Yb, Lu) and RuLn (Ln = Eu, Lu) helicates demonstrates that the heterobimetallic triple-helical complexes are rigid enough for providing comparable molecular structures for the d–f pairs, but flexible enough to tune the wrapping of the strands around metal ions of slightly different sizes. Although the long  $\text{M} \cdots \text{Ln}$  distance ( $d \geq 9.0 \text{ \AA}$ ) is only slightly affected by variation in the ionic radii of the host cations, it significantly depends on the intermetallic electrostatic repulsion, and it increases by about  $0.25 \text{ \AA}$  on going from  $[\text{RuLnL}_3]^{5+}$  to  $[\text{CrLnL}_3]^{6+}$ . Since the solution structures closely resemble those found in the solid state, we conclude that these discrete molecular objects are ideally suited for unravelling electrostatic multipolar interactions responsible for intramolecular intermetallic communication by  $nd \rightarrow 4f$  energy transfer, ultimately providing directional visible  $\rightarrow$  NIR light-converters. In this context, the d-block-centered deactivation rate constants in the absence of an acceptor ( $k_{\text{lum}}^{\text{M}}$ ), which differ by three orders of magnitude between  $\text{Cr}(^2\text{E})$  (millisecond range) and  $\text{Ru}(^3\text{MLCT})$  (microsecond range), are strictly mirrored in the rate of the  $nd \rightarrow 4f$  energy transfer process ( $k_{\text{ET}}^{\text{M,Ln}}$ ) with Ln = Nd, Er, Yb (Table 6). This somewhat unexpected behavior is responsible for the detection of significant, but incomplete intermetallic energy transfer when  $\text{Cr}^{\text{III}}$  or  $\text{Ru}^{\text{II}}$  are used as sensitizers. Moreover, these data suggest that both d-block-centered luminescence and energy transfer to the 4f acceptors are controlled by vibronic processes (i.e., phonon-assisted), which are more efficient for  $\text{Ru}(^3\text{MLCT})$  than for  $\text{Cr}(^2\text{E})$ . Finally, the critical radii  $R_0^{\text{M,Ln}}$ , calculated for each d–f pair, allow the prediction of the distance  $d_{\text{switch}}^{\text{M,Ln}}$ , at which  $k_{\text{ET}}^{\text{M,Ln}} = k_{\text{lum}}^{\text{Ln}}$  [Eq. (11)].

$$d_{\text{switch}}^{\text{M,Ln}} = R_0^{\text{M,Ln}} \cdot \sqrt[6]{\frac{k_{\text{lum}}^{\text{M}}}{k_{\text{lum}}^{\text{Ln}}}} \quad (11)$$

In other words,  $d_{\text{switch}}^{\text{M,Ln}}$  corresponds to the intermetallic separation for which the kinetic regime switches between NIR

emission reflecting the intrinsic lifetime of the Ln-centered excited state ( $k_{\text{ET}}^{\text{M,Ln}} > k_{\text{Lum}}^{\text{Ln}}$ , which translates into  $R_{\text{DA}} < d_{\text{switch}}^{\text{M,Ln}}$ ), and NIR luminescence decay driven by the population rate of the Ln excited level, that is, equal to the observed decay of the d-block sensitizer ( $k_{\text{ET}}^{\text{M,Ln}} < k_{\text{Lum}}^{\text{Ln}}$ , therefore  $R_{\text{DA}} > d_{\text{switch}}^{\text{M,Ln}}$ ). For  $[\text{CrLnL}_3]^{6+}$  (Ln=Nd, Yb),  $d_{\text{switch}}^{\text{Cr, Ln}} \approx 3.5\text{--}4.7 \text{ \AA}$  (Table 6) implies that apparent expansion of the NIR emission decay time is a common feature when a  $[\text{Cr}^{\text{III}}(\alpha, \alpha'\text{-diimine})_3]$  chromophore is used as a sensitizer for Ln=Nd and Yb in poly-metallic assemblies. However, a similar behavior with the  $[\text{Ru}^{\text{II}}(\alpha, \alpha'\text{-diimine})_3]$  chromophore requires larger separations ( $d_{\text{switch}}^{\text{Ru, Ln}} \approx 6\text{--}14 \text{ \AA}$ ), which may be a limiting factor for apparent Ln lifetime lengthening in RuLn bimetallic edifices. This controlled intermetallic communication offers promising perspectives for the design of novel homogeneous fluoroimmunoassays<sup>[1b]</sup> using time-resolved NIR luminescence, in which one monoclonal antibody is labelled with the d-block donor and the other one with the f-block acceptor.<sup>[31]</sup> Increased sensitivity is expected upon reaction with the specific target antigen and crucial structural information about the distance between the recognition sites becomes simultaneously accessible. This could also develop into a new tool for assessing distances between targeted sites in large biomolecules.

## Experimental Section

### Syntheses, solvents and starting materials:

These were purchased from Fluka AG (Buchs, Switzerland) and used without further purification unless otherwise stated. Acetonitrile was distilled from  $\text{CaH}_2$ . The complexes  $[\text{CrLnL}_3](\text{CF}_3\text{SO}_3)_6 \cdot x\text{H}_2\text{O}$  (Ln=Gd, Nd:  $x=6$ ; Ln=Yb:  $x=4$ ),<sup>[17]</sup>  $[\text{RuLnL}_3](\text{CF}_3\text{SO}_3)_5 \cdot x\text{H}_2\text{O} \cdot y\text{CH}_3\text{OH}$  (Ln=Nd:  $x=10$ ,  $y=1$ ; Ln=Eu:  $x=2$ ,  $y=2$ ; Ln=Gd: Er, Yb:  $x=6$ ,  $y=1$ )<sup>[19]</sup> and  $[\text{ZnLnL}_3](\text{CF}_3\text{SO}_3)_5 \cdot 3\text{H}_2\text{O}$  (Ln=Nd, Yb)<sup>[21]</sup> were prepared according to previously described procedures.

**Crystal structure of  $[\text{CrNdL}_3](\text{CF}_3\text{SO}_3)_6(\text{CH}_3\text{CN})_4(\text{H}_2\text{O})$  (5),  $[\text{CrYbL}_3](\text{CF}_3\text{SO}_3)_6(\text{CH}_3\text{CN})_4$  (7), and  $[\text{RuEuL}_3](\text{CF}_3\text{SO}_3)_5(\text{CH}_3\text{OH})_{1.5}(\text{H}_2\text{O})$  (9):** Summary of crystal data, intensity measurements, and structure refinements are collected in Table 7. All crystals were mounted on quartz fibers with protection oil. Cell dimensions and intensities were measured at 200 K on a Stoe IPDS diffractometer with graphite-monochromated  $\text{MoK}\alpha$  radiation ( $\lambda = 0.71073 \text{ \AA}$ ). Data were corrected for Lorentz and polarization effects and for absorption. The structures were solved by direct methods (SIR97),<sup>[32]</sup> all other calculations were performed with XTAL<sup>[33]</sup> system and ORTEP<sup>[34]</sup> programs. CCDC-220050 (5), CCDC-220051 (7), and CCDC-253390 (9) contain the

supplementary crystallographic data for this paper. These data can be obtained free of charge from The Cambridge Crystallographic Data Centre via [www.ccdc.cam.ac.uk/data\\_request/cif](http://www.ccdc.cam.ac.uk/data_request/cif).

Complexes 5 and 7 are isostructural with  $[\text{CrLnL}_3](\text{CF}_3\text{SO}_3)_6(\text{CH}_3\text{CN})_4$  (Ln=Eu, 6; Ln=Lu, 8).<sup>[17]</sup> The hydrogen atoms of the methyl groups were refined with restraints on bond lengths and angles, and blocked during the last cycles. The atomic positions of the other hydrogen atoms were calculated. In 5, the ethyl group C29b–C30b, the water molecule, and the triflate anions g and h are disordered and were refined on two sites with population parameters 0.5/0.5 for the ethyl and water molecule and 0.6/0.4 for each triflate anion.

The complex 9 is isostructural with  $[\text{RuLuL}_3](\text{CF}_3\text{SO}_3)_{4.5}\text{Cl}_{0.5}(\text{CH}_3\text{OH})_{2.5}$  (10).<sup>[19]</sup> The metric of the unit cell was not reduced ( $c < b$ ) to allow the same description of both isostructural structures. The ethyl group C29b–C30b, and the triflate anions f, g, and h were disordered and refined on two sites with population parameters 0.7/0.3 (ethyl, triflates f and g) and 0.75/0.25 (triflate h).

**Spectroscopic and analytical measurements:** IR spectra were obtained from KBr pellets with a Perkin–Elmer 883 spectrometer. Electronic spectra in the UV/Vis range were recorded at 20°C from acetonitrile solutions with a Perkin–Elmer Lambda 900 spectrometer using quartz cells of 0.1 and 1 cm path length. <sup>1</sup>H NMR spectra were recorded at 25°C on Bruker Avance 400 MHz and Bruker DRX-500 MHz spectrometers. Chemical shifts are given in ppm with respect to TMS. Pneumatically assisted electrospray (ESI-MS) mass spectra were recorded from  $10^{-4} \text{ mol dm}^{-3}$  solutions on a Finnigan SSQ7000 instrument. The equipment and experimental procedures for luminescence measurements in the visible range have been published previously.<sup>[35]</sup> Excitation of the finely powdered samples was achieved by a 450-W xenon high-pressure lamp coupled with a monochromator or a Coherent Innova Argon laser. The emitted light was analyzed at 90° with a Spex 1404 double monochromator with holographic gratings (band-path used 0.01–0.2 nm). Light intensity was measured by a RCA 31034 photomultiplier with a cooled S-

Table 7. Summary of crystal data, intensity measurement, and structure refinement for  $[\text{CrNdL}_3](\text{CF}_3\text{SO}_3)_6(\text{CH}_3\text{CN})_4(\text{H}_2\text{O})$  (5),  $[\text{CrYbL}_3](\text{CF}_3\text{SO}_3)_6(\text{CH}_3\text{CN})_4$  (7), and  $[\text{RuEuL}_3](\text{CF}_3\text{SO}_3)_5(\text{CH}_3\text{OH})_{1.5}(\text{H}_2\text{O})$  (9).

Compound	5	7	9
formula	$\text{C}_{113}\text{H}_{113}\text{CrNdN}_{25}\text{O}_{22}\text{F}_{18}\text{S}_6$	$\text{C}_{113}\text{H}_{111}\text{CrYbN}_{25}\text{O}_{21}\text{F}_{18}\text{S}_6$	$\text{C}_{105.5}\text{H}_{107}\text{RuEuN}_{21}\text{O}_{20.5}\text{F}_{15}\text{S}_5$
$M_r$	2904.1	2914.19	2695.7
crystal system	monoclinic	monoclinic	triclinic
space group	$P2_1/n$	$P2_1/n$	$P\bar{1}$
$a$ [ $\text{\AA}$ ]	22.2394(11)	22.2714(10)	17.8840(13)
$b$ [ $\text{\AA}$ ]	22.9564(9)	22.8851(12)	19.2523(13)
$c$ [ $\text{\AA}$ ]	24.6976(13)	24.3983(11)	19.0845(14)
$\alpha$ [ $^\circ$ ]			75.483(8)
$\beta$ [ $^\circ$ ]	92.002(6)	92.156(5)	79.772(9)
$\gamma$ [ $^\circ$ ]			69.999(8)
$V$ [ $\text{\AA}^3$ ]	12 601(1)	12 427(1)	5947.0(8)
$Z$	4	4	2
crystal size [mm]	$0.15 \times 0.22 \times 0.29$	$0.11 \times 0.17 \times 0.22$	$0.07 \times 0.16 \times 0.18$
$\rho_{\text{calcd}}$ [ $\text{Mg m}^{-3}$ ]	1.531	1.558	1.505
$\mu$ ( $\text{MoK}\alpha$ ) [ $\text{mm}^{-1}$ ]	0.697	1.041	0.84
$T_{\text{min}}, T_{\text{max}}$	0.8325, 0.9359	0.8211, 0.9108	0.8428, 0.9396
$2\theta_{\text{max}}$ [ $^\circ$ ]	51.8	53.8	51.7
no. of reflns collected	100 172	109 590	62 633
no. of independent reflns	24 506	25 870	21 561
no. of obsd <sup>[a]</sup> (used <sup>[b]</sup> )	12 492 (13 365)	11 648 (12 887)	8874 (9605)
reflns			
no. of variables	1841	1666	1554
weighting scheme $p$ <sup>[c]</sup>	0.0002	0.0002	0.00015
Max and min $\Delta\rho$ [ $\text{e \AA}^{-3}$ ]	1.03, -1.16	1.12, -1.01	1.58, -1.44
GOF ( $F$ ) <sup>[d]</sup> (all data)	1.17(1)	1.11(1)	0.96(1)
$R$ <sup>[e]</sup> , $\omega R$ <sup>[f]</sup>	0.047, 0.046	0.038, 0.037	0.048, 0.046

[a]  $|F_o| > 4\sigma(F_o)$ . [b] Used in the refinements (including reflns with  $|F_o| \leq 4\sigma(F_o)$  if  $|F_c| > |F_o|$ ). [c]  $\omega = 1/[\sigma^2(F_o) + p(F_o)^2]$ . [d]  $S = [\sum\{((F_o - F_c)/\sigma(F_o))^2 / (N_{\text{ref}} - N_{\text{var}})\}^{1/2}]$ . [e]  $R = \sum ||F_o| - |F_c|| / \sum |F_o|$ . [f]  $\omega R = [\sum(\omega |F_o| - |F_c|)^2 / \sum \omega |F_o|^2]^{1/2}$ .

20 photocathode ( $-20^{\circ}\text{C}$ ), coupled to a Lecroy linear amplifier (500 MHz) and a Stanford Research SR-400 double photon counter. For the emission in the NIR, light intensity was measured with a Jobin Yvon DSS-IGA020 L solid-state InGaAs detector cooled to 77 K, in a LN2 housing including an elliptical mirror ( $90^{\circ}$  beam path, range 800–1600 nm) and coupled to a Jobin Yvon SpectraAcq2 data acquisition system. The emission spectra were corrected for the instrumental function. The excitation spectra were corrected for the emission of the Xenon lamp. Luminescent lifetimes were measured by using excitation provided by a Quantum Brilliant Nd:YAG laser equipped with frequency doubler, tripler and quadrupler as well as with an OPOTEK MagicPrism OPO crystal. The output signal of the photomultiplier was fed into a Stanford Research SR-430 multichannel scaler and transferred to a PC. Lifetimes are averages of three independent determinations. To confirm that the measured lifetimes of the  $\text{Nd}^{\text{III}}$  and  $\text{Yb}^{\text{III}}$  emission are not biased by those of a residual emission of  $\text{Cr}^{\text{III}}$  or  $\text{Ru}^{\text{II}}$ , the CrEu and RuLu complexes were used as blanks. Quantum yields were determined by using a Spex Fluorolog 3–22 fluorimeter; for the ions emitting in the near infrared the spectrometer was fitted with an additional single grating monochromator FL-1004 equipped with an InGaAs detector cooled at 77 K. The quantum yields have been calculated by using Equation (12), where  $x$  refers to the sample and  $r$  to the reference;  $A$  is the absorbance (with  $A_x = A_r = 0.45 \pm 0.01$  ( $\text{Ru}^{\text{II}}$  and  $\text{Cr}^{\text{III}}$ ) or  $0.16 \pm 0.01$  ( $\text{Nd}^{\text{III}}$ ,  $\text{Yb}^{\text{III}}$ , and  $\text{Er}^{\text{III}}$ )),  $\bar{\nu}$  the excitation wavenumber used,  $I$  the intensity of the excitation light at this energy,  $n$  the refractive index and  $D$  the integrated emitted intensity.  $[\text{CrEuL}_3]^{6+}$  ( $\Phi = 0.13\%$ )<sup>[17]</sup> and  $[\text{RuLuL}_3]^{5+}$  ( $\Phi = 1.0\%$ )<sup>[19]</sup> were used as reference in acetonitrile for ions emitting in the visible region and  $\text{Yb}(\text{TTA})_3$  in toluene ( $\Phi = 0.35\%$ ; TTA = thenoyltrifluoroacetylacetonate)<sup>[37]</sup> for the NIR emitting ions (estimated error  $\pm 10\%$ ). Quartz Suprasil cells with 0.2 cm path length were used for these measurements. Elemental analyses were performed by Dr. H. Eder from the Microchemical Laboratory of the University of Geneva.

$$\frac{\Phi_x}{\Phi_r} = \frac{A_x(\bar{\nu})I_r(\bar{\nu})n_x^2D_x}{A_r(\bar{\nu})I_x(\bar{\nu})n_r^2D_r} \quad (12)$$

## Acknowledgements

We are grateful to Mr. Frédéric Gummy for his technical assistance in recording the luminescence data. This work was supported through grants from the Swiss National Science Foundation.

- [1] a) I. Hemmilä, T. Ståhlberg, P. Mottram, *Bioanalytical Applications of Labelling Technologies*, Wallac Oy: Turku, 1995; b) G. Mathis, *J. Biomol. Screen.* **1999**, *4*, 309; c) I. Hemmilä, V. M. Mikkala, *Crit. Rev. Clin. Lab. Sci.* **2001**, *38*, 441; d) S. Faulkner, J. L. Matthews in *Comprehensive Coordination Chemistry II* (Ed.: M. D. Ward), Elsevier, Oxford, UK, **2004**, pp. 913–944.
- [2] a) C. Reinhard, H. U. Güdel, *Inorg. Chem.* **2002**, *41*, 1048; b) A. Beeby, S. Faulkner, J. A. G. Williams, *J. Chem. Soc. Dalton Trans.* **2002**, 1918; c) R. van Deun, B. De Fré, D. Moors, K. Binnemans, *J. Mater. Chem.* **2003**, *13*, 1520; d) S. J. A. Pope, A. M. Kenwright, V. A. Boote, S. Faulkner, *Dalton Trans.* **2003**, 3780; e) G. M. Davies, R. J. Aarons, G. R. Motson, J. C. Jeffery, H. Adams, S. Faulkner, M. D. Ward, *Dalton Trans.* **2004**, 1136; f) S. Quici, G. Marzanni, A. Forni, G. Accorsi, F. Barigelletti, *Inorg. Chem.* **2004**, *43*, 1294; g) S. Faulkner, M.-C. Carrié, S. J. A. Pope, J. Squire, A. Beeby, P. G. Sammes, *Dalton Trans.* **2004**, 1405.
- [3] a) N. M. Shavaleev, S. J. A. Pope, Z. R. Bell, S. Faulkner, M. D. Ward, *Dalton Trans.* **2003**, 808; b) G. A. Hebbink, L. Grave, L. A. Woldering, D. N. Reinhoudt, F. C. J. M. van Veggel, *J. Phys. Chem. A* **2003**, *107*, 2483; c) T. J. Foley, B. S. Harrison, A. S. Kniefely, K. A. Abboud, J. R. Reynolds, K. S. Schanze, J. M. Boncella, *Inorg. Chem.* **2003**, *42*, 5023; d) H.-S. He, Z.-X. Zhao, W.-K. Wong, K.-F. Li, J.-X. Meng, K.-W. Cheah, *Dalton Trans.* **2003**, 980; e) H. He, J. Guo, Z.-X. Zhao, W.-K. Wong, W.-Y. Wong, W.-K. Lo, K.-F. Li, K.-W. Cheah, *Eur. J. Inorg. Chem.* **2004**, 837.
- [4] a) S. I. Klink, H. Keizer, F. C. J. M. van Veggel, *Angew. Chem.* **2000**, *112*, 4489; *Angew. Chem. Int. Ed.* **2000**, *39*, 4319; b) P. D. Beer, F. Szemes, P. Passaniti, M. Maestri, *Inorg. Chem.* **2004**, *43*, 3965; c) S. J. A. Pope, B. J. Coe, S. Faulkner, E. V. Bichenkova, X. Yu, K. T. Douglas, *J. Am. Chem. Soc.* **2004**, *126*, 9490; d) T. A. Miller, J. C. Jeffery, M. D. Ward, H. Adams, S. J. A. Pope, S. Faulkner, *Dalton Trans.* **2004**, 1524.
- [5] a) N. M. Shavaleev, L. P. Moorcraft, S. J. A. Pope, Z. R. Bell, S. Faulkner, M. D. Ward, *Chem. Commun.* **2003**, 1134; b) N. M. Shavaleev, L. P. Moorcraft, S. J. A. Pope, Z. R. Bell, S. Faulkner, M. D. Ward, *Chem. Eur. J.* **2003**, *9*, 5283; c) P. B. Glover, P. R. Ashton, L. J. Childs, A. Rodger, M. Kercher, R. M. Williams, L. De Cola, Z. Pikramenou, *J. Am. Chem. Soc.* **2003**, *125*, 9918.
- [6] S. J. A. Pope, B. J. Coe, S. Faulkner, *Chem. Commun.* **2004**, 1550.
- [7] M. A. Subhan, H. Nakata, T. Suzuki, J.-H. Choi, S. Kaizaki, *J. Lumin.* **2003**, *101*, 307.
- [8] a) P. R. Contag, I. N. Olomu, D. K. Stevenson, C. H. Contag, *Nat. Med.* **1998**, *4*, 245; b) S. Bhaumik, S. S. Gambhir, *Proc. Natl. Acad. Sci. USA* **2002**, *99*, 377; c) S. Kim, Y. T. Lim, E. G. Soltész, A. M. De Grand, J. Lee, A. Nakayama, J. A. Parker, T. Mihajljevic, R. G. Laurence, D. M. Dor, L. H. Cohn, M. G. Bawendi, J. V. Frangioni, *Nat. Biotechnol.* **2004**, *22*, 93.
- [9] M. H. V. Werts, R. H. Woudenberg, P. G. Emmerink, R. van Gassel, J. W. Hofstraat, J. W. Verhoeven, *Angew. Chem.* **2000**, *112*, 4716; *Angew. Chem. Int. Ed.* **2000**, *39*, 4542.
- [10] R. Reisfeld, C. K. Jørgensen, *Lasers and Excited States of Rare Earths*, Springer, Heidelberg, **1977**.
- [11] a) Y. Oshishi, T. Kanamori, Y. Kitagawa, S. Takashashi, E. Snitzer, G. H. Sigel Jr., *Opt. Lett.* **1991**, *16*, 1747; b) R. J. Mears, S. R. Baker, *Opt. Quantum Electron.* **1992**, *24*, 517; c) E. Desurvire, *Phys. Today* **1994**, *47*, 20.
- [12] a) T. Förster in *Comparative Effects of Radiation* (Eds.: M. Burton, J. S. Kirby-Smith, J. L. Magee), Wiley, New York, **1960**, pp. 300–319; b) D. L. Dexter, *J. Chem. Phys.* **1953**, *21*, 836.
- [13] a) W. de W. Horrocks Jr., J. P. Bolender, W. D. Smith, R. M. Supkowski, *J. Am. Chem. Soc.* **1997**, *119*, 5972; b) R. M. Supkowski, J. P. Bolender, W. D. Smith, L. E. L. Reynold, W. de W. Horrocks Jr., *Coord. Chem. Rev.* **1999**, *185–186*, 307.
- [14] J.-C. G. Bünzli, C. Piguet, *Chem. Rev.* **2002**, *102*, 1897.
- [15] For reviews, see a) A. Juris, V. Balzani, F. Barigelletti, S. Campagna, P. Belser, A. von Zelewsky, *Coord. Chem. Rev.* **1988**, *84*, 85; b) E. C. Constable, *Adv. Inorg. Chem.* **1989**, *34*, 1; c) V. Balzani, A. Juris, S. Venturi, S. Campagna, S. Serroni, *Chem. Rev.* **1996**, *96*, 759; d) J. F. Endicott, B. H. Schlegel, Md. J. Uddin, D. S. Seniveratne, *Coord. Chem. Rev.* **2002**, *229*, 95.
- [16] J.-C. G. Bünzli In *Lanthanide Probes in Life, Chemical and Earth Sciences* (Eds.: J.-C. G. Bünzli, G. R. Choppin), Elsevier, Amsterdam, **1989**, Chapter 7.
- [17] M. Cantuel, G. Bernardinelli, D. Imbert, J.-C. G. Bünzli, G. Hopfgartner, C. Piguet, *J. Chem. Soc. Dalton Trans.* **2002**, 1929.
- [18] D. Imbert, M. Cantuel, J.-C. G. Bünzli, G. Bernardinelli, C. Piguet, *J. Am. Chem. Soc.* **2003**, *125*, 15698.
- [19] S. Torelli, S. Delahaye, A. Hauser, G. Bernardinelli, C. Piguet, *Chem. Eur. J.* **2004**, *10*, 3503.
- [20] a) J.-M. Lehn, *Supramolecular Chemistry*, VCH, Weinheim, **1995**; b) C. Piguet, G. Bernardinelli, G. Hopfgartner, *Chem. Rev.* **1997**, *97*, 2005.
- [21] C. Piguet, J.-C. G. Bünzli, G. Bernardinelli, G. Hopfgartner, S. Petoud, O. Schaad, *J. Am. Chem. Soc.* **1996**, *118*, 6681.
- [22] R. D. Shannon, *Acta Crystallogr. Sect. A* **1976**, *32*, 751.
- [23] C. Piguet, G. Bernardinelli, B. Bocquet, O. Schaad, and A. F. Williams, *Inorg. Chem.* **1994**, *33*, 4112.
- [24] C. Piguet, J.-C. G. Bünzli, G. Bernardinelli, C. G. Bochet, and P. Froidevaux, *J. Chem. Soc. Dalton Trans.* **1995**, 83.
- [25] S. Rigault, C. Piguet, G. Bernardinelli, and G. Hopfgartner, *J. Chem. Soc. Dalton Trans.* **2000**, 4587.

- [26] M. Cantuel, G. Bernardinelli, G. Muller, J. P. Riehl, C. Piguet, *Inorg. Chem.* **2004**, *43*, 1840.
- [27] W. T. Carnall, P. R. Fields, K. Rajnak, *J. Chem. Phys.* **1968**, *49*, 4443.
- [28] F. R. Gonçalves e Silva, O. L. Malta, C. Reinhard, H. U. Güdel, C. Piguet, J. E. Moser, J.-C. G. Bünzli, *J. Phys. Chem. A* **2002**, *106*, 1670.
- [29] M. E. Starzak, *Mathematical Methods in Chemistry and Physics*, Plenum Press, New York, **1989**, Chapter 6, pp. 300–309.
- [30] The decay rate constant  $k$  of an excited state is related to its characteristic lifetime  $\tau$  by  $k = \tau^{-1}$ .
- [31] G. Mathis in *Rare Earths* (Eds.: R. Saez Puche, P. A. Caro), Editorial Complutense, Madrid, **1998**, pp. 285–298.
- [32] A. Altomare, M. C. Burla, M. Camalli, G. Cascarano, C. Giacovazzo, A. Guagliardi, A. G. G. Moliterni, G. Polidori, R. Spagna, *J. Appl. Crystallogr.* **1999**, *32*, 115.
- [33] *XTAL 3.2 User's Manual* (Eds.: S. R. Hall, H. D. Flack, J. M. Stewart), Universities of Western Australia and Maryland, **1989**.
- [34] C. K. Johnson, *ORTEP II; Report ORNL-5138*, Oak Ridge National Laboratory, Oak Ridge, Tennessee, **1976**.
- [35] R. Rodriguez-Cortinas, F. Avecilla, C. Platas-Iglesias, D. Imbert, J.-C. G. Bünzli, A. de Blas, T. Rodriguez-Blas, *Inorg. Chem.* **2002**, *41*, 5336.
- [36] a) J. H. Brewster, *Top. Curr. Chem.* **1974**, *47*, 29; b) F. Renaud, C. Piguet, G. Bernardinelli, J.-C. G. Bünzli, G. Hopfgartner, *J. Am. Chem. Soc.* **1999**, *121*, 9326.
- [37] S. B. Meshkova, Z. M. Topilova, D. V. Bolshoy, S. V. Beltyukova, M. P. Tsvirko, V. Y. Venchikov, *Acta Phys. Pol. A* **1999**, *95*, 983.

Received: November 17, 2004  
Published online: March 18, 2005